A central role for regulated protein stability in the control of TFE3 and MITF by nutrients

Christopher Nardone[1,2], **Brad A. Palanski**[3], **Daniel C. Scott**[4], **Richard T. Timms**[5], **Karl W. Barber**[1,2], **Xin Gu**[6], **Aoyue Mao**[1,2], **Yumei Leng**[1,2], **Emma V. Watson**[1,2], **Brenda A. Schulman**[7], **Philip A. Cole**[3], **Stephen J. Elledge**[1,2,8,*]

[1]Division of Genetics, Department of Medicine, Howard Hughes Medical Institute, Brigham and Women's Hospital, Boston, MA 02115, USA

[2]Department of Genetics, Harvard Medical School, Boston, MA 02115, USA

[3]Division of Genetics, Department of Medicine, Brigham and Women's Hospital; Department of Biological Chemistry and Molecular Pharmacology, Harvard Medical School, Boston, MA 02115, USA

[4]Department of Structural Biology, St. Jude Children's Research Hospital, Memphis, TN 38105, USA

[5]Cambridge Institute of Therapeutic Immunology and Infectious Disease, Department of Medicine, University of Cambridge, Jeffrey Cheah Biomedical Centre, Puddicombe Way, Cambridge, Cambridgeshire CB2 0AW, UK

[6]Department of Neurobiology, Harvard Medical School, Boston, MA 02115, USA

[7]Department of Molecular Machines and Signaling, Max Planck Institute of Biochemistry, Martinsried, 82152, Germany

[8]Lead contact

SUMMARY

The TFE3 and MITF master transcription factors maintain metabolic homeostasis by regulating lysosomal, melanocytic, and autophagy genes. Previous studies posited that their cytosolic retention by 14–3–3, mediated by the Rag GTPases-mTORC1, was key for suppressing transcriptional activity in the presence of nutrients. Here, we demonstrate using mammalian cells that regulated protein stability plays a fundamental role in their control. Amino acids

promote the recruitment of TFE3 and MITF to the lysosomal surface via the Rag GTPases, activating an evolutionarily conserved phospho-degron leading to ubiquitination by CUL1$^{\beta\text{-TrCP}}$ and degradation. Elucidation of the minimal functional degron revealed a conserved alpha-helix required for interaction with RagA, illuminating the molecular basis for a severe neurodevelopmental syndrome caused by missense mutations in *TFE3* within the RagA-TFE3 interface. Additionally, the phospho-degron is recurrently lost in *TFE3* genomic translocations that cause kidney cancer. Therefore, two divergent pathologies converge on the loss of protein stability regulation by nutrients.

Graphical Abstract
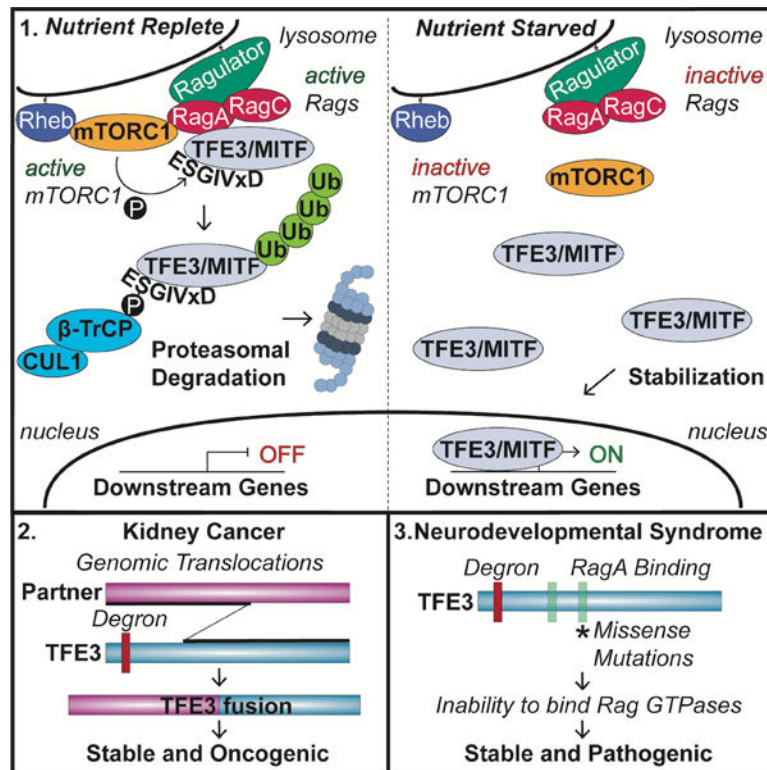
Blurb

Nardone et al. elucidate a fundamental role for regulated protein degradation to control the activity of the key lysosomal and melanosomal transcription factors, TFE3 and MITF. Genomic rearrangements or missense mutations of TFE3 can lead to constitutive stabilization and activation, resulting in a severe kidney cancer or neurodevelopmental syndrome, respectively.

Keywords

TFE3; MITF; ubiquitin; β-TrCP; nutrient-sensing; lysosomes; Rag GTPases; mTORC1; phosphodegron; kidney cancer; neurodevelopment

INTRODUCTION

Selective protein degradation is a critical mechanism by which the regulation of gene expression is achieved. Many important mediators of development, tumor suppression, cell cycle regulation, and signal transduction are selectively targeted for degradation, and thus disrupting this process can lead to a wide range of human diseases.[1] A key strategy through which to execute broad transcriptional programs is by selectively tuning the abundance of transcription factors. This occurs largely through the 26S proteasome when polyubiquitin chains are conjugated to protein substrates through the sequential action of the ubiquitin (Ub) activating enzyme (E1), Ub conjugating enzymes (E2), and Ub ligases (E3). Over 600 E3 ligases confer substrate specificity by recognizing amino acid sequence motifs that act as degradation signals (degrons).[2,3] Crucial transcription factors, such as HIF2α, NRF2, and MYC are selectively targeted for degradation and this regulation is important for physiology and pathology.[4–6] However, if and how the many other transcription factors are selectively targeted for protein degradation has not been systematically explored on a proteome-wide level. Here, we leverage an unbiased, high-throughput method of quantifying protein stability in human cells to identify transcription factors targeted for protein degradation by cullin-RING ligases (CRLs), a family encompassing one-third of all E3 ligases.

From our efforts detailed below, we identify that TFE3 and MITF are strikingly unstable proteins. They, together with TFEB and TFEC, comprise the MiT/TFE family of basic helix-loop-helix leucine zippers which bind to DNA as homo- or hetero-dimers that play crucial roles in the maintenance of cellular energy homeostasis.[7,8] MITF acts as a master regulator of melanocyte survival and differentiation as well as melanosome biogenesis by binding M-box motifs present in the promoter region of pigmentation genes.[9,10] In contrast, TFE3 and TFEB act as master regulators of lysosomal biogenesis and autophagy through binding a modified E-box called the CLEAR element for Coordinated Lysosomal Expression And Regulation.[11–13] For example, the CLEAR element is enriched in the promoter region of v-ATPase subunits, lysosomal membrane proteins, lysosomal hydrolases, and autophagy adaptors. The physiological importance is underscored by the fact that missense mutations and genomic rearrangement events in *TFE3* cause a severe neurodevelopmental syndrome and kidney cancer, respectively.[14–17] Despite their established roles in health and disease, the upstream regulation of TFE3 and MITF, and the molecular basis for these pathologies remain elusive.

Previous studies established a role for the essential nutrient-sensing Rag GTPases-mTORC1 pathway in the regulation of the MiT/TFE family.[18–21] These factors are recruited to the lysosomal surface in the presence of amino acids by interacting with active Rag GTPases, leading to phosphorylation by mTORC1 (mechanistic Target Of Rapamycin Complex 1), a kinase complex that functions as the master regulator of cell growth.[22,23] This phosphorylation event creates a binding site for the 14-3-3 chaperone proteins that sequester the transcription factors in the cytosol. Current literature hypothesizes that 14-3-3 mediated retention is the key event that suppresses transcriptional activity.[24] The importance of the MiT/TFE family at a cellular and organismal level prompted our investigation of how and why TFE3 and MITF were potently regulated by a protein degradation pathway.

RESULTS

A GPS ORFeome screen identifies unstable transcription factors targeted for degradation by cullin-RING ligases

The work described utilized a high-throughput method of quantifying protein stability called Global Protein Stability (GPS), a lentiviral fluorescence reporter system.[25,26] GPS transcripts are bicistronic and encode DsRed as an internal control, followed by GFP fused to a human open reading frame (ORF) that is translated from an upstream internal-ribosome-entry-site (IRES). The relative stability of the fusion protein is determined by quantifying the ratio of GFP/DsRed via flow cytometry (Figure 1A). We previously established a barcoded library that contains ~15,000 human ORFs in the GPS vector (GPS ORFeome) that can be harnessed to assess changes in protein stability on a proteome-wide level.[27] We screened the GPS ORFeome library in the presence and absence of a potent and specific inhibitor of cullin-RING ligase activation, MLN4924, to determine how CRLs may regulate the stability of transcription factors on a proteome-wide level (Figure 1A). MLN4924 inhibits a process referred to as NEDDylation, which is essential for ubiquitination activity of CRLs.[28] This screen was analyzed specifically for known or predicted transcription factors (Table S1).[29] A variety of transcription factors known to be canonically regulated by CRLs exhibited significant stabilization upon treatment with MLN4924, including HIF2α and MYC. Owing to the physiological and pathological importance, we focused on TFE3 and MITF (Figure 1B).

To validate the results of the GPS ORFeome screen, TFE3, TFEB, and three variants of MITF were tagged at the N-terminus with GFP using the lentiviral GPS system and expressed in human embryonic kidney (HEK)-293T cells. Treatment with MLN4924 strongly increased the stability of TFE3 and the longest, ubiquitously expressed isoform of MITF (MITF-A, variant 1), whereas no change was observed for TFEB and two shorter, tissue-specific variants of MITF (MITF-M and MITF-5) that lack an N-terminal region present within MITF-A (Figure 1C). Immunoblotting was then performed using validated antibodies to examine whether the corresponding endogenous proteins were similarly affected (Figure S1A). The steady state abundance of both TFE3 and MITF increased substantially upon addition of MLN4924 without similarly affecting their mRNA expression (Figure S1B) or mTORC1 signaling (Figure S1C), while no significant change was observed for TFEB (Figure 1D). A similar effect on protein abundance was also observed in adult retinal pigment epithelial (ARPE)-19 cells (Figure S1D and S1E).

TFE3 and MITF-A are targeted for proteasomal degradation by CUL1β-TrCP1/2

Cullin-RING-ligases are modular protein complexes defined by a conserved scaffold of one of several Cullin (CUL) isoforms, each of which utilizes a unique set of substrate-receptor proteins that directly deliver substrates to the Cullin for ubiquitination. To determine which Cullin was responsible for the degradation, individual dominant-negative Cullin proteins were expressed in HEK-293T cells harboring the GPS TFE3 reporter.[27] Only dominant-negative CUL1 increased the stability of TFE3 (Figure 1E) and MITF-A (Figure 1F); thus, TFE3 and MITF-A are putative CUL1 substrates.

CUL1 utilizes SKP1 to recruit a set of 69 unique F-box substrate-receptor proteins that deliver substrates for ubiquitination.[30] We performed a CRISPR-Cas9 screen using a curated library of guide RNAs targeting genes related to the ubiquitin-proteasome system to uncover the putative F-box substrate-receptor (Figure 2A). As anticipated, the top scoring genes from this screen were CUL1 and SKP1, the NEDDylation machinery, and many proteasomal subunits (Figure 2B and Table S2), the latter supported by stabilization of both TFE3 and MITF-A by the proteasome inhibitor Bortezomib (Figure S1F). Among the top scoring genes was β-TrCP2, which recognizes the same phospho-degron as its paralog β-TrCP1.[31]

To validate the screen results, three different siRNA were used to deplete the two β-TrCP paralogs. Depletion of β-TrCP1 did not stabilize TFE3 or MITF-A; however, depletion of β-TrCP2 did stabilize both transcription factors and the β-TrCP1/2 double depletion resulted in further stabilization, phenocopying the effects of MLN4924 and dominant-negative CUL1 (Figure 2C, S1G, and S1H). Furthermore, immunoprecipitation of FLAG-tagged TFE3 and MITF-A followed by immunoblotting revealed a robust interaction with endogenous β-TrCP1 (Figure 2D). Reciprocal immunoprecipitation of FLAG-tagged β-TrCP1/2 revealed a strong interaction with endogenous TFE3 and MITF-A, but not TFEB, consistent with the latter lacking regulation by CUL1$^{\beta\text{-TrCP1/2}}$ (Figure 2E). In addition, mutagenesis of critical residues within the β-TrCP1 substrate recognition WD40 domain previously shown to be necessary for interaction with β-catenin[32] abolished the interaction with TFE3 and MITF-A (Figure 2F). Altogether, these results indicate that TFE3 and MITF-A are targeted for proteasomal degradation by CUL1$^{\beta\text{-TrCP1/2}}$.

Phosphorylation of a conserved degron in TFE3 and MITF-A is necessary for ubiquitination by CUL1$^{\beta\text{-TrCP1/2}}$

We examined the amino acid sequences of the MiT/TFE family members to determine if TFE3 and MITF-A contain a motif resembling the consensus β-TrCP1/2 degron, D(pS)Gxx(pS), where (pS) indicates phosphoserine. Indeed, TFE3 and MITF-A, but not TFEB or the melanocytic MITF-M, contain an ESGIVxD motif near their N-terminus (Figure 3A). Whereas mutagenesis of nearby residues had minimal effects, substitution of residues within this putative degron strongly stabilized both transcription factors, and no further stabilization was observed upon addition of MLN4924 (Figure 3B).

β-TrCP1/2-mediated recognition of degrons containing serine or threonine residues requires their phosphorylation.[33] Thus, we hypothesized the ESGIVxD motif is phosphorylated, and that this modification is required for ubiquitination of TFE3 and MITF-A by CUL1$^{\beta\text{-TrCP1/2}}$. To determine if the serine residue within the degron is phosphorylated, FLAG-tagged TFE3 and MITF-A were immunoprecipitated from HEK-293T cells that were treated with MLN4924 to increase the abundance of the phosphorylated species and digested with trypsin. Phosphopeptides were enriched by immobilized metal affinity chromatography for identification by liquid chromatography-tandem mass spectrometry (LC-MS/MS). Analysis of MITF-A phosphopeptides suggested that the degron serine (underlined) within the tryptic peptide AGTMQSESGIVPDFEVGEEFHEEPK is phosphorylated (Figure 3C, S2A, and Table S3). Peptide standards were then used to confirm the identity of the tryptic peptide and the localization of the phosphosite (Figure S2B). To enable tryptic digestion of a

peptide spanning the degron, an S42R substitution was introduced to TFE3 that does not significantly alter protein stability and remains stabilized by MLN4924 (Figure S3A). LC-MS/MS analysis following phospho-enrichment of TFE3[S42R] tryptic peptides demonstrated that the degron serine (underlined) within LLPE_S_GIVADIELENVLDPDSFYELK is phosphorylated and synthetic peptide standards were again used to confirm the identity of the extracted phosphopeptide (Figure S3B, S3C, and Table S3). Thus, the degron serine residue of TFE3 (S47) and MITF-A (S5) is phosphorylated in cells.

To determine if the phospho-degron is sufficient to permit the interaction between β-TrCP1/2 and the transcription factors, we synthesized biotinylated synthetic peptides spanning the degron with and without serine phosphorylation. We performed streptavidin pull down assays using lysates from cells expressing FLAG-tagged β-TrCP1/2. Notably, only the phosphorylated forms of the TFE3 and MITF-A peptides interacted with β-TrCP1/2 (Figure 3D). Moreover, only the phosphorylated forms of the degron peptides were ubiquitinated *in vitro* using a reconstituted NEDDylated CUL1[β-TrCP2] complex and blocking the C-terminal lysine residue using biotin abolished the ubiquitination of the phosphopeptides (Figure 3E).

Mutagenesis of S47 and S5 within the degron of TFE3 and MITF-A, respectively, completely abolished the interaction with endogenous β-TrCP1 (Figure 3F). To test directly if phosphorylation of the degron is necessary for ubiquitination, full-length native and degron phosphorylated (pS5)-MITF-A were isolated using a genomically recoded *E. coli* organism that incorporates phosphoserine in place of the UAG stop codon (Figure S4A, S4B, S4C, and Table S4).[34] MITF-A was rapidly ubiquitinated by the reconstituted NEDDylated CUL1[β-TrCP2] complex *in vitro* only when the degron serine residue was selectively phosphorylated (Figure 3G). The β-TrCP1/2 degron within TFE3 and MITF-A is highly conserved during evolution from *Drosophila melanogaster* and *Hydra vulgaris* to humans, suggesting this newfound degradative pathway may be important for metazoan physiology (Figure 3H). Thus, TFE3 and MITF-A require phosphorylation of a single serine residue within a conserved degron for interaction with and ubiquitination by CUL1[β-TrCP1/2].

Active Rag GTPases promote CUL1[β-TrCP1/2]-dependent degradation

Having established that TFE3 and MITF-A are targeted for proteasomal degradation by CUL1[β-TrCP1/2] in a phosphorylation-dependent manner, we next set out to determine the kinase responsible. To do this, we repeated the CRISPR-Cas9 screens to identify mutants which stabilize TFE3 and MITF-A, except that this time a genome-wide library of CRISPR sgRNAs was employed. Reassuringly, many positive controls were strongly enriched, including CUL1, SKP1, the NEDDylation machinery, and numerous proteasomal subunits. Interestingly, many components of the amino acid sensing Rag GTPases-mTORC1 pathway scored as prominent hits (Figure 4A and Table S5), including positive regulators of mTORC1 signaling such as the v-ATPase subunits, FLCN-FNIP1/2, the heteropentameric Ragulator complex (LAMTOR1–5), RagA, components of the GATOR2 complex (WDR59, WDR23, and SEH1L), and mTORC1 (MTOR and RPTOR) itself.

mTORC1 activity is tightly regulated by small GTPases localized at the lysosomal surface. In the presence of amino acids, mTORC1 is recruited to the lysosomal surface by the Rag

GTPases and Ragulator (LAMTOR1–5), a heteropentameric complex that anchors the Rag GTPases to the lysosome.[35–37] Once recruited, the kinase activity of mTORC1 is activated by Rheb, another small GTPase that is directly anchored to the lysosomal membrane.[38,39] The Rag proteins function as obligate heterodimers in which the active complex consists of RagA or B bound to GTP and RagC or D bound to GDP. The presence of amino acids keeps the Rag heterodimers in the active state, thereby promoting the recruitment of the mTORC1 complex. However, in the absence of amino acids, the Rag GTPases are turned to the inactive GDP-bound Rag A or B and GTP-bound Rag C or D, thereby inactivating mTORC1 by promoting its cytosolic redistribution. Like mTORC1, the MiT/TFE family is recruited to the lysosomal surface in the presence of amino acids by interacting with Rag GTPases.[18–21] This leads to phosphorylation within a conserved serine residue and subsequent cytosolic sequestration by 14-3-3 chaperones. Given that no other protein kinase enriched strongly between both screens, we hypothesized that TFE3 and MITF-A are recruited to the lysosomal surface by interacting with active Rag GTPases, resulting in phosphorylation of the degron serine residue by mTORC1 and subsequent ubiquitination by $CUL1^{\beta\text{-TrCP1/2}}$.

We employed RagA/B, RagC/D, and LAMTOR1 knockout (KO) HEK-293T cells to test this hypothesis.[40] The steady state abundance of endogenous TFE3 and MITF-A was greater in the RagA/B, RagC/D, and LAMTOR1 KO cells relative to wild type by immunoblotting (Figure 4B). GPS reporter cells for TFE3 and MITF-A were established in these KO backgrounds and indeed the transcription factors were substantially more stable in the KO cells relative to wild type (Figure 4C and S4D). Crucially, the addition of MLN4924 did not further stabilize the transcription factors, suggesting that the Rag GTPases-mTORC1 pathway lies upstream of the degradation by $CUL1^{\beta\text{-TrCP1/2}}$. Complementation of RagC/D KO cells with constitutively active- but not inactive-RagC restored the degradation by $CUL1^{\beta\text{-TrCP1/2}}$, consistent with the notion that these transcription factors interact with active Rag GTPases (Figure S4E).[20] A region within the MiT/TFE family was previously shown to be important for mediating the interaction with Rag GTPases (Rag Binding Domain).[20] Deletion of this region within TFE3 and MITF-A abrogated the interaction with Rag GTPases and β-TrCP1, suggesting loss of degron phosphorylation (Figure 4D). Additionally, deletion of the Rag binding domain, or mutagenesis of key residues within it, sharply increased the stability of both transcription factors and the addition of MLN4924 did not further stabilize the transcription factor mutants (Figure 4E). Therefore, these results support the hypothesis that the Rag GTPases regulate $CUL1^{\beta\text{-TrCP1/2}}$-dependent degradation likely by modulating degron phosphorylation via recruitment to the lysosomal surface.

Control of TFE3 and MITF-A degradation by nutrients is crucial to suppress transcriptional activity

We next tested the role of nutrients in modulating degron phosphorylation via the mTORC1 pathway. Amino acid and serum starvation or mTORC1 inhibition with Torin1 increased the steady state abundance of endogenous TFE3 and MITF-A (Figure 5A), consistent with a reduction in protein degradation, and abolished the interaction between the transcription factors and β-TrCP1 (Figure 5B), consistent with a reduction in degron phosphorylation. The reciprocal immunoprecipitation of β-TrCP1/2 also demonstrated that the interaction

with both transcription factors was completely abolished by Torin1 treatment, further supporting that degron phosphorylation may be dependent upon mTORC1 activity, directly or indirectly (Figure 5C).

Given that the MiT/TFE family is sequestered by 14-3-3 chaperones, we wanted to determine whether their protein degradation is dependent on their binding to 14-3-3. Previous work established that mutagenesis of S321 and S280 within TFE3 and MITF-A, respectively, increases their nuclear localization and entirely abolishes their retention by 14-3-3 chaperones.[13,41] However, TFE3 and MITF-A remained unstable after mutagenesis of these key serine residues, and in fact these mutants have lower abundance than the wild type proteins, suggesting the nuclear environment is more destabilizing than the cytosol (Figure 5D). To further examine this, the nuclear localization sequence within TFE3 was mutagenized and this mutant remained entirely cytoplasmic even in the presence of Torin1 (Figure S5A).[42] This NLS mutant was more stable than the wild type protein, consistent with the nuclear environment being destabilizing, and the addition of MLN4924 still stabilized this TFE3 mutant (Figure S5A). Thus, TFE3 remains degraded independent of its ability to translocate within the nucleus. Additionally, treatment of TFE3^{S321A} cells with Torin1 still promoted stabilization (Figure S5B). Therefore, the degradative pathway that is regulated by phosphorylation of S47 (TFE3) and S5 (MITF-A) operates in parallel to the cytoplasmic retention by 14-3-3 that is regulated by phosphorylation of S321 (TFE3) and S280 (MITF-A).

Next, we assessed the transcriptional activity of TFE3 and MITF-A to tease apart how the newfound degradative pathway integrates with the cytoplasmic retention by 14-3-3. A dual luciferase reporter under the control of 4xCLEAR or 3xM-box motifs was stably introduced into TFE3/MITF-A double KO HEK-293T cells through lentiviral transduction, and luciferase expression was determined after complementation with wild type or mutant versions of the transcription factors (Figure S5C). Reconstitution with constitutively stable TFE3^{S47A} increased luciferase expression relative to the wild type protein (Figure 5E). In contrast, expression of TFE3^{S321A} did not upregulate gene expression, consistent with the possibility that, due to its increased instability, its levels are too low in the nucleus to promote transcription (Figure S5D). However, complementation with the double TFE3$^{S47A/S321A}$ mutant that is both refractory to degradation and 14-3-3 retention showed that the two mutants had a cooperative effect. Furthermore, the inability to bind Rag GTPases resulted in a further increase in transcriptional activity, consistent with the likelihood that additional phosphosite(s) may regulate nuclear translocation (Figure S5D).[13,24] A similar trend was observed for MITF-A (Figure 5F). Since the luciferase experiment utilizes multiple transcription factor binding sites that might not report on endogenous targets in a fully representative manner, we performed a similar experiment by examining the expression of endogenous TFE3 and MITF target genes.[10,43] Consistent with the luciferase data, the effect of removing the 14-3-3 regulation is only seen when TFE3 and MITF are constitutively stable and therefore stabilization plays a central role for the activation of bonafide endogenous transcriptional targets of both TFE3 and MITF (Figure S5E). Cumulatively, these results support the notion that stabilization of TFE3 and MITF-A is both necessary and partially sufficient to upregulate downstream gene transcription.

TFE3 is aberrantly stabilized in translocation renal cell carcinoma

Xp11.2 translocation renal cell carcinoma (tRCC) is a unique type of kidney cancer caused by genomic rearrangements of *TFE3* normally located on chromosome Xp11.2.[17] The translocation event involves a breakpoint within *TFE3*, leading to the expression of oncogenic fusion proteins in which a C-terminal portion of TFE3 is fused to the N-terminal portion of a variety of partners. Clinical studies have reported numerous TFE3 fusion partners, and one recently reported case also identified a PRCC-MITF fusion.[44–64] Compellingly, the β-TrCP1/2 degron within TFE3 and MITF-A is lost during the translocation event in almost all of these clinically reported cases (Figure 6A). Indeed, MiT/TFE oncogenic fusions observed in the clinic are significantly more stable than the corresponding wild type transcription factor (Figure 6B and Figure S6A). To test if the degradation of the fusion protein is restored upon reintroduction of the degron, we engineered NONO-TFE3 fusions in which truncated NONO was fused to full-length wild type or mutant versions of TFE3. Full-length NONO-TFE3 (WT) displayed substantially reduced expression compared to the truncated NONO-TFE3 observed clinically (Figure 6C). However, the expression level of the full-length TFE3 fusion was restored to the levels of the truncated oncogenic NONO-TFE3 upon mutagenesis of the phospho-degron (S47A) or the Rag binding domain (S112A/R113A). Therefore, degron loss is key to establish a stable, high expressing oncogenic fusion protein.

A neurodevelopmental syndrome is caused by mutations in TFE3 within a RagA interface

The definition of the required β-TrCP1/2 phospho-degron motif within TFE3 and MITF-A is clear but, unlike most degrons, it does not appear to confer instability when transferred to another protein. We performed a truncation analysis using MITF-A to determine which region of the protein was sufficient for the degradation to occur. We suspected that a C-terminally truncated MITF-A construct (residues 1–120) that retained the β-TrCP1/2 degron and the currently defined Rag binding domain (henceforth called helix 1) would provide regulated destruction, but it was not degraded by $CUL1^{\beta-TrCP1/2}$ (Figure S6B). However, a slightly larger MITF-A construct (residues 1–163) did confer regulated stability and, by inference, phosphorylation. To investigate whether these additional 43 amino acids formed any recognizable structure, we examined its structure prediction by AlphaFold which indicated that this additional segment folds into an alpha helix (henceforth called helix 2) that is highly conserved among MiT/TFE family members (Figure 6D and S6C).[65]

This helix 2 region, which appeared essential for the stability regulation, is associated with a severe human disease. *De novo* mutations within *TFE3* were recently identified in patients suffering from a neurodevelopmental syndrome with pigmentation defects.[14–16] Almost all of these mutations are missense and occur in two regions: a few mutations were identified within helix 1, but the majority were located within or immediately adjacent to helix 2 (Figure 6D). Therefore, we hypothesized that this elusive helix 2 region may be necessary for interaction with Rag GTPases and degron phosphorylation.

To test this hypothesis, we introduced the neurological syndrome patient mutations into TFE3. All mutations potently stabilized TFE3 (Figure 6E) and similar results were observed for the corresponding mutations in MITF-A (Figure S7A). Importantly, all the examined

mutants abolished binding to Rag GTPases and β-TrCP1, consistent with a reduction in degron phosphorylation (Figure 6F). The corresponding mutations in MITF-A and TFEB similarly abrogated the interaction with Rag GTPases, indicating a crucial role for this region in lysosomal surface recruitment (Figure S7B and S7C). These results suggested that both helix 1 and helix 2 are necessary for MiT/TFE family members to interact with Rag GTPases. We were curious as to whether these two regions are sufficient to confer binding to Rag GTPases. Immunoprecipitation of helix 1 fused to GFP revealed that it alone was not sufficient to mediate the interaction, while helix 2 alone did interact weakly with endogenous Rag GTPases (Figure 6G). However, the interaction with Rag GTPases was robustly restored when both helix 1 and helix 2 were together fused to GFP. Thus, both helices are necessary and sufficient for interaction with Rag GTPases, demonstrating how MiT/TFE family members are recruited to the lysosomal surface.

To gain insight into the possible docking mechanism, we employed ColabFold to predict the structure of the helix 1+2 region of TFE3 bound to RagA and RagC.[66] While no interaction was observed for helix 1, we found that the helix 2 area clearly docks onto a region of RagA that forms an extensive interface with the neurodevelopmental syndrome associated residues of TFE3 (Figure 7A). Inspection of this interface revealed that the key residues within RagA that establish salt bridge or hydrogen bonding interactions with TFE3 were E71, E100, H104, Q107, E111, L151, R153, and P154 (Figure 7B). To validate this finding, we generated alanine mutations in or around these critical residues and the RagA mutants were expressed in RagA/B KO cells. While mutagenesis of nearby residues had negligible effects on interaction, mutagenesis of the critical residues potently abolished the interaction between RagA and TFE3 or TFEB, without affecting the ability of RagA to bind Raptor or heterodimerize with RagC (Figure 7C). Additionally, mutagenesis of RagA within its switch I or interswitch regions (Y31 and D35/E46), abolished the interaction with Raptor as shown previously[40] while only mildly affecting the recruitment of TFE3/TFEB. Finally, expression of constitutively active RagA in RagA/B KO cells restored the degradation of TFE3 while the crucial interface RagA mutants were unable to do the same (Figure S7D). We thus conclude that the MiT/TFE family members are recruited to the Rag GTPases at the lysosomal surface, at least partially, via direct interaction with RagA.

DISCUSSION

The governance of master regulatory programs is complex and often incorporates multiple layers of control including signal transduction, transcriptional, translational, post-transcriptional, and post-translational modes of regulation. Here, in hopes of uncovering new layers of regulation, we examined the post-translational control of transcription factors by the ubiquitin-proteasome system using GPS. We uncovered a large collection of TFs that are under the control of cullin-RING-ligases, which are known to couple signal transduction and protein stability, that serves as a resource for future investigation. Among these, we focused on two related transcription factors. TFE3 and MITF-A are responsible for maintaining metabolic homeostasis in response to nutrient availability. To achieve this, these factors promote a coordinated transcriptional program that is responsible for the expression of lysosomal, autophagic, and melanocytic genes, among many others. Owing to their crucial roles, their transcriptional activity must be exquisitely controlled such that

activation occurs largely in response to metabolic stress. Appropriately, the activity of the MiT/TFE family is directly regulated by the Rag GTPases, which are at the center of an essential nutrient-sensing pathway that promotes anabolism while suppressing catabolism via a master protein kinase, mTORC1. The MiT/TFE family interacts with the Rag GTPases and are phosphorylated by mTORC1, leading to cytosolic sequestration. Previous studies posited that their cytoplasmic retention by 14-3-3 was the key regulatory event governing their activity.[24] Here, however, we show that regulated protein degradation appears to play an even more critical role in the control of TFE3 and MITF-A by nutrients.

Our efforts revealed that TFE3 and MITF-A are recruited to the lysosomal surface by interacting with Rag GTPases and are phosphorylated at a serine residue within an evolutionarily conserved degron in the presence of amino acids (Figure 7D). This phosphorylation event creates an active degron that is targeted by CUL1$^{\beta\text{-TrCP1/2}}$, resulting in ubiquitination and subsequent proteasomal degradation. This degradation pathway is indispensable for suppressing the activity of TFE3 and MITF-A. Loss of the cytoplasmic retention by 14-3-3 alone is not sufficient to activate TFE3 and MITF-A, as they likely remain too unstable to accumulate within the nucleus. However, their stabilization is a crucial event that is both necessary and partially sufficient to upregulate downstream transcription of CLEAR and M-box containing genes. We propose that active Rag GTPases regulate TFE3 and MITF-A in multiple layers to exquisitely control their transcriptional activity. The fundamental, outermost layer of regulation promotes protein degradation and stabilization must occur to further activate TFE3 and MITF-A via other mechanisms such as nuclear translocation. This regulation is logical as these transcription factors largely promote catabolic processes such as autophagy and oxidative metabolism, which requires suppression in the presence of nutrients. Interestingly, loss of TFE3 alone in ARPE-19 cells completely abrogates the expression of lysosomal and autophagy genes during starvation.[13]

Why TFE3 and MITF-A, but not TFEB, are co-regulated by this important evolutionarily conserved degradative pathway is unknown. A previous study found that mice lacking TFE3 and MITF develop severe osteopetrosis, a phenotype that is unique to the germline double knockout.[67] This finding suggests that TFE3 and MITF may act cooperatively or redundantly to regulate a defined set of genes. Stabilization of TFE3 and MITF-A during nutrient deprivation increases the abundance of both transcription factors and may shift the equilibrium to a hetero-dimeric state. It is intriguing to speculate that a TFE3/MITF-A hetero-dimer may promote a unique transcriptional program as a crucial response to the scarcity of nutrients.

The importance of this degradative regulation is underscored by the fact that aberrant stabilization of TFE3 and MITF-A occurs in multiple human diseases. Among these is translocation renal cell carcinoma, which accounts for most pediatric and up to 5% of adult renal cell carcinomas.[68] This aggressive cancer is caused by a genomic rearrangement event of the MiT/TFE family, most commonly TFE3, resulting in the production of an oncogenic truncated fusion protein with recurring fusion boundaries, the basis for which was unknown. We found that the β-TrCP1/2 degron within TFE3 and MITF-A is recurrently lost in clinically reported cases (Figure 7E). Interestingly, several TFE3 fusions selectively lose the β-TrCP1/2 degron but retain the ability to bind Rag GTPases, thus

these fusions retain the 14-3-3 cytosolic retention pathway. Given that stabilization is crucial for transcriptional activity of TFE3 and MITF-A, this finding suggests a key driver for the disease is stabilization of what would otherwise be an unstable fusion protein. Numerous mechanisms may exist that determine the oncogenicity of fusion proteins, such as transcriptional upregulation due to promoter exchange.[69] However, we found the high expression of the fusion protein is critically determined via loss of the protein degradation pathway uncovered in this study. More work modeling Xp11.2 tRCC at an organismal level is warranted to understand the tissue specificity, the cell-type of origin, and how stabilization contributes to onset of this aggressive disease.

Beyond cancer, missense mutations within *TFE3* have been reported to cause a neurodevelopmental syndrome with pigmentation defects.[14–16] Patients suffering from this disease exhibit severe neurological symptoms such as intellectual disability and epilepsy, with all affected individuals being non-verbal. Despite the serious developmental defects, the molecular basis for this disorder was unknown. Most of the reported missense mutations cluster in an evolutionarily conserved domain. Upon inspection of the ClinVar database, we found several additional individuals containing missense mutations within this same hotspot region that were unclassified, likely due to a small sample size at the time of whole-exome sequencing. Serendipitously, we found this elusive domain was critical for the regulation of protein degradation. We show that the disease-associated missense mutations abolish the ability to interact with Rag GTPases and constitutively stabilize TFE3. Furthermore, the previously defined Rag binding domain (helix 1) together with the disease-associated alpha helix (helix 2) is both necessary and sufficient to interact with Rag GTPases. Using ColabFold to predict how this region interacts with the Rag GTPases, we found and extensively validated that the MiT/TFE family docks onto a region of RagA. Most importantly, the patient-derived mutations occur at this RagA-TFE3 interface and mutagenesis of the interacting RagA residues phenocopy the patient-derived mutations with respect to binding and stabilization of TFE3. While it remains unclear how helix 1 contributes to the binding, these results establish the molecular basis for a severe neurodevelopmental syndrome caused by mutations in *TFE3* and more clearly define how the MiT/TFE family is recruited to the lysosomal surface by the Rag GTPases (Figure 7F).

These insights may prove invaluable in the development of novel therapeutics. Gain of function experiments demonstrated that TFE3/TFEB promote clearance of toxic protein aggregates, exocytosis of damaged lysosomes, and lipid oxidation to rescue a mouse model of fatty liver disease.[11,13,70] Thus, the ability to selectively activate the MiT/TFE family in nutrient-replete conditions, without globally affecting the Rag GTPase-mTORC1 pathway, could have broad untapped therapeutic implications. Small molecules or peptides that abrogate the interaction interface between RagA and the MiT/TFE family could be an attractive starting point.

Limitations of the Study:

The interaction between TFE3/MITF and β-TrCP1/2 requires degron phosphorylation. Thus, we monitor the degron phosphorylation status by probing for the interaction between the TFE3/MITF with β-TrCP1/2. While we use mass spectrometry to show the degron serine

residue of TFE3 and MITF is unequivocally phosphorylated in cells, establishing a phospho-specific antibody for this site will be crucial for future work to study the dynamics of this phosphosite. We provide circumstantial evidence that mTORC1 may be the kinase responsible for degron phosphorylation, but we do not show it may directly do so. Future *in vitro* reconstitution assays should be performed using purified Rag GTPases, mTORC1, and MiT/TFE family members to determine the directness of the kinase. Finally, we performed a structure prediction of TFE3 with RagA/C using ColabFold to establish a direct role of RagA in interacting with MiT/TFE family members. We acknowledge this is a predicted structure with partial verification, and future work will be required to understand how MiT/TFE family members may also interact with RagC or Raptor (mTORC1).

STAR Methods

RESOURCE AVAILABILITY

Lead Contact—Further information and request for reagents should be directed to and will be fulfilled by the lead contact, Stephen J. Elledge (selledge@genetics.med.harvard.edu).

Materials Availability—Any reagents that are unique to this study will be made available upon request.

Data and Code Availability

- Raw images and mass spectrometry files were deposited to Mendeley Data and were made public as of the date of publication. The DOI is listed in the Key Resources Table.

- Detailed GPS ORFeome, CRISPR-Cas9 screens, and mass spectrometry data are available in Tables S1, S2, S3, S4, and S5.

- This paper does not report original code.

- Any additional information necessary to reanalyze the data reported in this paper is available from the lead contact upon request.

EXPERIMENTAL MODEL AND SUBJECT DETAILS

Cell culture

HEK-293T (ATCC, CRL-3216) and NIH/3T3 cells (ATCC, CRL-1658) were cultured in Dulbecco's Modified Eagle's Medium (DMEM) (Thermo Fisher Scientific, 11965118) supplemented with 10% fetal bovine serum (Cytiva, SH30088.03) and 100 units/mL of penicillin and 0.1 mg/mL of streptomycin (Thermo Fisher Scientific, 15070063). ARPE-19 cells (ATCC, CRL-2302) were cultured in a 1:1 mixture of DMEM and Ham's F12 medium (Thermo Fisher Scientific, 11320082) supplemented with 10% fetal bovine serum and 100 units/mL of penicillin and 0.1 mg/mL of streptomycin. All cells were cultured at 37°C and 5% CO_2. For chemical treatments, cells were treated for 24 hours unless stated otherwise with 1 μM MLN4924 (Selleckchem, S7109), 10 μM Bortezomib (APExBIO, A2614), or 500 nM Torin1 (TOCRIS, 4247) from 1000x stock solutions in DMSO. For amino acid/

serum starvation, cells were washed twice with PBS and cultured for 24 hours unless stated otherwise with RPMI lacking amino acids (USBiological, R9010–01) and serum.

METHOD DETAILS

Lentivirus production

To generate lentiviral stocks, HEK-293T cells were transfected using PolyJet (SignaGen, SL100688) following the manufacturer's instructions with lentiviral transfer vector and plasmids encoding Tat, Rev, Gag-Pol, and VSV-G. Fresh media was added to cells post transfection and the lentiviral supernatant was collected 48 hours later, passed through a 0.45 µm filter, and applied onto cells dropwise or stored at -80°C for future use.

Plasmids

The barcoded GPS ORFeome expression library containing about 15,000 human ORFs was generated previously [27]. A custom sgRNA library targeting the ubiquitin-proteasome system (ubiquitome) (6 sgRNAs/gene, 9,230 sgRNAs total) was used.[74] The sgRNA information for this curated library can be found in Table S2. The genome wide CRISPR sgRNA Root library (5 sgRNAs/gene, 94,335 sgRNAs total) was used.[75] The sgRNA information for this genome wide library can be found in Table S5. Plasmids encoding the cDNAs for TFE3 (IOH14020), MITF-A (IOH52183), MITF-M (IOH45654), MITF-5 (IOH22837), TFEB (IOH21660), β-TrCP1 (IOH11366), β-TrCP2 (IOH11042), NONO (IOH5111), ASPSCR1 (IOH13970), and PRCC (IOH5200) were obtained in the form of entry clones from the Ultimate ORF Clone collection (Thermo Fisher Scientific). The cDNA for RagA (Addgene, 73031) and RagC (Addgene, 99718) was obtained, PCR amplified with attB1/2 overhangs, and cloned into the pDONR221 (Thermo Fisher Scientific, 12536017) via a BP recombination reaction (Thermo Fisher Scientific, 11789020) to generate the entry clone. Primers were designed using the NEBaseChanger program and entry clones were mutagenized or truncated by PCR following the Q5 Site Directed Mutagenesis kit (NEB, E0554S).

TFE3 and MITF fusion entry clones were generated by overlap extension PCR. The information regarding the fusion boundaries used to generate Figure 6A was obtained from the primary literature.[44–64]

Entry clones were subcloned into lentiviral pHAGE-CMV-FLAG-HA[27], pHAGE-GPS 3.0[27], or pHAGE-EF1α[72] Gateway Destination vectors via an LR recombination reaction (Thermo Fisher Scientific, 11791100). Dominant-negative Cullin constructs originated as a kind gift from W. Harper.[27] TFE3 helices fused to GFP-FLAG were generated by synthesis where helix1 of TFE3 encoded the amino acid region 106–140, helix2 180–210, and helix1+2 106–210. For CRISPR-Cas9 experiments to generate clonal knockouts, sgRNAs were cloned into lentiCRISPRv2 (Addgene, 52961) using BsmBI (NEB, R0739S) to digest the backbone, followed by phosphorylation and annealing of guideRNA oligos containing CACC or AAAC overhangs obtained from IDT, and T4 (NEB, M0202S) ligation. For dual luciferase experiments, pHAGE-5xISRE-ffLuc-PGK-renLuc was generated previously.[73] This plasmid was digested with NheI (NEB, R3131S) and XhoI (NEB, R0146L) to excise

the 5xISRE. Oligos containing the following motifs were obtained from IDT with NheI or XhoI overhangs for subsequent T4 ligation into the digested dual luciferase plasmid.

4xCLEAR:
GTAGGCCACGTGACCGGGGTAGGCCACGTGACCGGGGTAGGCCACGTGACCGGG
GTAGGCCACGTGACCGGGC

3xM-box:
AAAAGTCAGTCATGTGCTTTTCAAAAGTCAGTCATGTGCTTTTCAAAAGTCAGTC
ATGTGCTTTTC

DNA encoding human MITF-A was codon optimized for expression in *E. coli* K12 using the IDT codon optimization tool and inserted into the pdCas9-bacteria plasmid (Addgene, 44249)[84] replacing the dCas9 sequence. The encoded serine residue at position 5 in MITF-A was replaced with a TAG codon to enable co-translational incorporation of phosphoserine (pSer)[71] or serine using SepOTS (V70) (Addgene, 68292) or supD (Addgene, 68307)[85] plasmid-based amber suppression systems, respectively.[34,86,87]

Isolation of recombinant MITF-A

The engineered pMITF-A-bacteria plasmid was transformed into genomically recoded *E. coli* lacking genomic TAG codons (rEcoli^{XpS})[71] for expression[88]. Transformed cells were recovered for 1 hour in 1 mL LB at 37°C and 230 rpm and then directly inoculated in 100 mL LB + 25 μg/mL chloramphenicol + 50 μg/mL kanamycin and grown at 37 °C and 230 rpm for 16 hours. Cells from these precultures were then diluted to $OD_{600} = 0.2$ in 250 mL LB supplemented with 25 μg/mL chloramphenicol and 50 μg/mL kanamycin. Cells were grown at 37°C and 230 rpm for ~4 hours until $OD_{600} = 0.8$. MITF expression was induced using 100 ng/mL anhydrotetracycline and grown for an additional 4 hours at 30°C and 230 rpm. Harvested cell pellets were stored at − 80°C for at least 16 hours.

Cell pellets were thawed at 37°C. Each pellet was resuspended in 25 mL lysis buffer composed of 50 mM Tris pH 7.5, 500 mM NaCl, 10% glycerol, 100 μM DTT, 5 μL rLysozyme solution (Millipore Sigma, 71110–4), 50 μL benzonase (90% purity, Millipore Sigma, 70746–3), 1x BugBuster (Millipore Sigma, 70921–4), 1x cOmplete EDTA-free protease inhibitor cocktail (Millipore Sigma, 5892953001), 50 mM NaF, and 1 mM Na_3VO_4. The cells were incubated in the lysis buffer at 25°C for 20 minutes, mixing end-over-end. Lysates were clarified by spinning cells at 5,000xg for 20 minutes, and supernatant was transferred to 500 μL bed volume equilibrated Ni-NTA agarose (Qiagen, 30210). The clarified lysate was incubated with the resin for 20 minutes at 25°C and then the resin was washed twice with 10 mL wash buffer (50 mM Tris pH 7.4, 500 mM NaCl, 10% glycerol, 100 μM DTT, 20 mM imidazole). MITF was then eluted using 2 x 500 μL elution buffer (50 mM Tris pH 7.4, 500 mM NaCl, 10% glycerol, 100 μM DTT, 500 mM imidazole) and buffer exchanged using an Amicon Ultra-4 30 kDa molecular weight cutoff centrifugal filter (Millipore Sigma, UFC803024) three times using 4 mL storage buffer (25 mM HEPES pH 7.5, 200 mM NaCl, 1 mM DTT). The protein was concentrated to a final volume of 50–100 μL. The protein isolation was validated by trypsin digestion and analysis

of peptides by LC-MS/MS to validate the identity of the extracted native and pS5-MITF-A proteins.

Flow cytometry

Cells were rinsed once with PBS and detached using 0.05% trypsin and analyzed on a BD LSRII instrument (Becton Dickinson) or on a CytoFLEX S flow cytometer (Beckman Coulter, V2-B2-Y3-R2 version #C09762). The BD FACS Diva software (Becton Dickinson) or CytExpert software (Beckman Coulter) were used to collect flow cytometry data that was then analyzed using the FlowJo software. Fluorescence-activated cell sorting (FACS) was performed on either a Sony MA900 or a MoFlo Astrios (Beckman Coulter) instrument.

GPS ORFeome screen

GPS expression screens with the human ORFeome library were performed as described previously with minor modifications.[27] Briefly, the plasmid library (containing ~15,000 barcoded human ORFs fused to GFP) was packaged into lentiviral particles through the transfection of HEK-293T cells using PolyJet. HEK-293T cells were then transduced at a multiplicity of infection (MOI) of ~0.3, with puromycin selection (1.5 μg/mL for 4 days) commencing 48 hours post-transduction used to remove untransduced cells. On day 7 post-transduction, the cells were partitioned into six stability bins based on the GFP/DsRed ratio by FACS using a MoFlo Astrios instrument (Beckman Coulter). The sorting gates were established using control (DMSO-treated) cells such that ~1/6th of the population fell into each bin; the same settings were maintained for the subsequent sorting of the MLN4924-treated population (1 μM for 8 hours). Sufficient cell numbers were used at each step to ensure at least 100-fold representation of the library was maintained throughout.

CRISPR-Cas9 screens

CRISPR-Cas9 screens to identify genes responsible for regulating protein stability were performed as described previously.[27] Two different plasmid libraries were used. The ubiquitome CRISPR library was used to uncover the F-box substrate receptor. The genome-wide CRISPR Root library was used to uncover other upstream stability regulators more comprehensively. Briefly, the plasmid library was packaged into lentiviral particles through transfection of HEK-293T cells using PolyJet. HEK-293T cells stably expressing GPS TFE3 or MITF-A reporters were transduced with library virus at an MOI of ~0.3 and selected with puromycin (2 μg/mL for 7 days) starting 48 hours post-transduction to remove untransduced cells. On day 9 post-transduction, the cells were partitioned into the 95th percentile most stable population based on the GFP/DsRed ratio by FACS using a MoFlo Astrios instrument (Beckman Coulter). An unsorted input population was collected based on the number of cells collected in the 95th percentile. Sufficient cell numbers were used at each step to ensure at least 500-fold representation of the library was maintained throughout.

Generating knockout cells

DNA oligos were cloned as single guide RNAs into the lentiCRISPRv2 vector containing BFP as a fluorescence marker as described earlier. The following sgRNAs were used to generate TFE3/MITF double knockout HEK-293T cells:

sgTFE3 – GTTCATCGAGGGTCTTGCTG

sg1-MITF – GCCACATACAGCAAGCCCAA

sg2-MITF - GGTACCTTAAGGACTTCCAT

HEK-293T cells were transfected with the cloned lentiCRISPRv2 BFP plasmids using Polyjet. To generate TFE3/MITF double knockout, the plasmids were co-transfected. About 4–5 days post-transfection, the BFP-positive cells were single-cell sorted by FACS into 96-well plates. The cells were allowed to grow as single clones for about 2 weeks before further expanding and screening for knockout. Two different TFE3/MITF clones were isolated that demonstrated complete loss of expression by immunoblotting.

siRNA knockdown

HEK-293T cells were seeded at 250,000 cells/well in a 6-well plate and incubated overnight. The following day, the media was changed 1 hour before transfection using 1.5 mL of media per well. The media used contained FBS/antibiotics. siRNAs obtained from Dharmacon were reconstituted using 1x siRNA buffer (Dharmacon, B-002000-UB-100) to obtain a 20 μM stock solution. The following siRNA were used:

Non-targeting Control (Dharmacon, D-001810-01-05)

Non-targeting Control (Dharmacon, D-001810-02-05)

Non-targeting Control (Dharmacon, D-001810-03-05)

β-TrCP1 (Dharmacon, J-003463-05-0005)

β-TrCP1 (Dharmacon, J-003463-06-0005)

β-TrCP1 (Dharmacon, J-003463-07-0005)

β-TrCP2 (Dharmacon, J-003490-05-0005)

β-TrCP2 (Dharmacon, J-003490-06-0005)

β-TrCP2 (Dharmacon, J-003490-07-0005)

Then, 6 μL of individual siRNA (20 μM) was diluted in 250 μL of Opti-MEM media (Thermo Fisher Scientific, 31985070) lacking FBS/antibiotics and briefly vortexed to mix gently. For double depletion experiments, 6 μL of each individual siRNA was added in combination. 5 μL of Lipofectamine RNAiMAX (Thermo Fisher Scientific, 13778075) was diluted in 250 μL of Opti-MEM media lacking FBS/antibiotics. The RNAiMAX solution was immediately mixed with the siRNA solution to obtain a 500 μL solution of the siRNA-RNAiMAX solution. Mixture was briefly vortexed and incubated at room temperature for 18 minutes to allow the complex to form. The entire 500 μL solution was added to cells to obtain a final siRNA concentration of at least 60 nM and incubated overnight. The following day, the media was changed media and gene expression was assayed around 72 hours post transfection.

Immunoprecipitation

HEK-293T cells were cultured in 15 cm culture plates. Cells stably expressing the indicated constructs were generated by lentivirus using an MOI of ~0.2. Alternatively, cells were transiently transfected with 8 μg of the indicated plasmid DNA when ~60% confluent using PolyJet. If transfected, the media was changed the following day and replaced with fresh media in the presence and absence of indicated perturbations. Cells were rinsed once with ice cold PBS and harvested by scraping in 1 mL of buffer containing 25 mM HEPES pH 7.4, 150 mM NaCl, 5 mM EDTA, and 1% Triton X-100 supplemented with 1x protease and phosphatase inhibitor cocktail (Thermo Fisher Scientific, 78441). Cell lysates were incubated at 4°C with end-to-end rotation for 30 minutes. Cell lysates were centrifuged at 21,000xg for 15 minutes at 4°C. While centrifuging, anti-FLAG magnetic beads (Sigma, M8823) or anti-HA magnetic beads (Thermo Fisher Scientific, 88836) were washed 3 times in lysis buffer, using 15 μL of beads for every 15 cm plate harvested. An input aliquot of the supernatant was collected for further analysis by immunoblotting. Then, the beads were incubated with the remaining supernatant for 2 hours at 4°C with end-to-end rotation. The immunoprecipitates were washed three times with lysis buffer. The beads and input were resuspended in Tris-Glycine SDS sample buffer (Thermo Fisher Scientific, LC2676) containing 10% 2-mercaptoethanol and the protein was eluted by heating at 95°C for 5 minutes.

Immunoblotting

For determining differences in steady-state abundances, cells were rinsed once with PBS and lysed for 15 minutes at 4°C with rocking using RIPA buffer (Boston BioProducts, BP-115X) supplemented with 1x protease and phosphatase inhibitor cocktail (Thermo Fisher Scientific, 78441). Cell lysates were centrifuged at 21,000xg for 15 minutes at 4°C. The supernatant was collected, protein concentrations normalized using a BCA protein assay kit (Thermo Fisher Scientific, 23225), and diluted in Tris-Glycine SDS sample buffer for analysis by immunoblotting. Samples from immunoprecipitates were run directly for analysis by immunoblotting. Protein was loaded into 4–12% Tris-Glycine 15-well pre-cast gels (Thermo Fisher Scientific, XP04125BOX) and electrophoresis was conducted in 1x Tris-Glycine SDS running buffer (Thermo Fisher Scientific, LC2675–4) at a constant 180 v until the molecular weight ladder reached the bottom of the gel. A 10 to 250 kDa molecular weight ladder was used as a reference (Thermo Fisher Scientific, 26619). The protein in the gel was transferred to a 0.2 μm nitrocellulose membrane (BioRad, 170–4158) using the Trans-Blot Turbo Transfer System (BioRad). Membranes were blocked in 5% milk (LabScientific, M-0842) diluted in 1x TBST (SantaCruz, sc-36231) for at least 30 minutes at room temperature. The following primary antibodies were applied at a 1:1000 dilution directly in the blocking solution for overnight incubation at 4°C with rocking: rabbit polyclonal anti-TFE3 (Sigma, HPA023881), rabbit monoclonal anti-MITF (CST, 97800), rabbit polyclonal anti-TFEB (CST, 4240), rabbit monoclonal anti-Actin (CST, 4970), rabbit monoclonal anti-β-TrCP1 (CST, 4394), rabbit monoclonal anti-FLAG (CST, 14793), mouse monoclonal anti-FLAG (Sigma, F1804), rabbit monoclonal anti-HA (CST, 3724), rabbit monoclonal anti-RagA (CST, 4357), rabbit polyclonal anti-RagC (CST, 3360), rabbit polyclonal anti-Raptor (Sigma, 09–217), rabbit monoclonal anti-LAMTOR1 (CST, 8975), rabbit monoclonal anti-S6 Ribosomal Protein (CST, 2217), rabbit polyclonal

anti-Phospho-S6 Ribosomal Protein (CST, 2211), or rabbit monoclonal anti-His tag (CST, 12698). After overnight incubation, membranes were rinsed thoroughly using 1x TBST to remove residual primary antibody. Then, 5% milk in 1x TBST was again added to the membranes containing a 1:2000 dilution of the following secondary antibody for 1 hour incubation at room temperature with rocking: goat anti-Rabbit IgG (H+L), HRP conjugate (Thermo Fisher Scientific, 31460) or goat anti-Mouse IgG (H+L), HRP conjugate (Thermo Fisher Scientific, 31430). After incubation with secondary antibody, membranes were rinsed thoroughly using 1x TBST and exposed to either Pierce ECL western blotting substrate (Thermo Fisher Scientific, 32106) for easily detectable proteins, or Immobilon western chemiluminescent HRP substrate (Sigma, WBKLS0500) for lower abundant or more difficult to detect proteins. For most of the immunoblotting data presented, data was collected by exposing blots to high sensitivity autoradiography film (Denville Scientific, E3218). For Figure S4A, the data was collected using an Odyssey XF Li-COR.

In vitro ubiquitination

UBE2D2, UBE2M, ubiquitin, NEDD8, and the NEDD8 E1 NAE1-UBA3 were expressed in *E. coli* BL21 Gold (DE3) cells as GST-Thrombin fusion proteins and purified as described previously.[89] Full-length CUL1-RBX1, the ubiquitin E1 UBA1, and full-length SKP1-β-TrCP2 complex were expressed in insect cells as GST-TEV fusion proteins and purified as described previously.[89] NEDDylation and purification of NEDD8~CUL1–RBX1 was prepared as described previously.[90] To introduce a cysteine for fluorescent labeling of ubiquitin we mutated the protein kinase a site in the pGEX2TK backbone converting the PKA site from RRASV to RRACV.[90]

In vitro ubiquitination assays utilized a pulse-chase format.[91] Briefly, AlexaFluor-labeled ubiquitin (referred to as *ubiquitin) was thioester-linked to UBE2D2 in a "pulse" reaction incubating 10 μM UBE2D2, 15 μM *ubiquitin, and 400 nM UBA1 in 25 mM HEPES, 200 mM NaCl, 2.5 mM $MgCl_2$, 1 mM ATP, pH 7.5 for 15 minutes at room temperature. The pulse reaction was quenched for 5 minutes on ice with 50 mM EDTA, and *ubiquitin was chased from UBE2D2 to SCF substrates. Chase reactions consisted of mixing the E2~*ubiquitin thioester conjugate (75 nM final concentration) with NEDD8~CUL1-RBX1 (100 nM final concentration) pre-incubated with or without SKP1-β-TrCP2 (100 nM final concentration) and the indicated test substrates (125 nM final concentration). Reactions were performed on ice in 25 mM MES, 100 mM NaCl, 50 mM EDTA, 1 mg/mL BSA, pH 6.5. Aliquots were quenched at the indicated times by mixing with SDS sample buffer, separated by SDS-PAGE, and analyzed based on fluorescent signal of *ubiquitin using a Typhoon FLA9500 Phosphoimager (GE Healthcare). Test substrates included the recombinant native and phosphorylated MITF-A described earlier. The following peptide substrates were utilized (pS = phosphoserine):

Macromolecular Synthesis Lab, St. Jude

p-IκBα: Acetyl-KERLLDDRHD(pS)GLD(pS)MRDEERRASY

Elim Biopharmaceuticals, Inc.

TFE3: LLPESGIVADIELENVLDPDSFYELK

p-TFE3: LLPE(pS)GIVADIELENVLDPDSFYELK

TFE3-biotin: LLPESGIVADIELENVLDPDSFYELK-biotin

p-TFE3-biotin: LLPE(pS)GIVADIELENVLDPDSFYELK-biotin

MITF-A: AGTMQSESGIVPDFEVGEEFHEEPK

p-MITF-A: AGTMQSE(pS)GIVPDFEVGEEFHEEPK

MITF-A-biotin: MQSESGIVPDFEVGEEFHEEPK-biotin

p-MITF-A-biotin: MQSE(pS)GIVPDFEVGEEFHEEPK-biotin

Peptide pulldowns

Streptavidin magnetic beads (Thermo Fisher Scientific, 88816) were equilibrated in lysis buffer containing 20 mM HEPES pH 7.5, 150 mM NaCl, and 0.5% Triton X-100 containing protease and phosphatase inhibitor cocktail. About 15 μL of beads were used per peptide condition and 400 μL of lysis buffer was added to the beads. The biotinylated native or phosphorylated synthetic peptides spanning the degron region of TFE3 and MITF-A as described above were immobilized by adding 20 μg of peptide directly to the lysis buffer containing streptavidin beads. Peptides were incubated with the streptavidin beads for 1 hour at 4°C with end-to-end rotation. During this incubation step, HEK-293T cells cultured on 15 cm plates transiently expressing FLAG-tagged β-TrCP1 or β-TrCP2 were harvested using the same buffer by cell scraping. Cells were lysed by end-to-end rotation for 30 minutes at 4°C and then centrifuged at 21,000xg for 15 minutes at 4°C. A small aliquot of supernatant was collected for the input cell lysate. Once the peptides equilibrated with streptavidin beads, the beads were rinsed once with lysis buffer. The cell lysate for each β-TrCP paralog was split evenly and added directly onto the native or phosphorylated immobilized peptides. The mixture was incubated with end-to-end rotation for 2 hours at 4°C. The beads were rinsed 3 times with lysis buffer following incubation and resuspended in Tris-Glycine SDS sample buffer containing 10% 2-mercaptoethanol. The protein was eluted by heating at 95°C for 5 minutes.

Phosphoenrichment

To enable tryptic digestion of TFE3 spanning the degron, an S42R mutation was introduced within the cDNA using SDM as described earlier. The stability of this mutant was tested using the GPS reporter in the presence and absence of 1 μM MLN4924 for 24 hours. HEK-293T cells were established to stably express FLAG-HA-TFE3^{S42R} or FLAG-HA-MITF-A^{WT} using lentivirus. Cells were grown to 80% confluency in 30 15 cm plates for each transcription factor and then were treated with 1 μM MLN4924 for 24 hours to increase the abundance of the phosphorylated species. Cells in plates were harvested and lysed in buffer containing 25 mM HEPES pH 7.4, 150 mM NaCl, 5 mM EDTA, and 1% Triton X-100 supplemented with protease and phosphatase inhibitor cocktail. Cell lysates were incubated at 4°C with end-to-end rotation for 30 minutes. Cell lysates were centrifuged

at 21,000xg for 15 minutes at 4°C. While centrifuging, anti-FLAG magnetic beads were washed 3 times in lysis buffer, using 15 μL of beads for every 15 cm plate harvested. The anti-FLAG beads were incubated with the supernatant for 2 hours at 4°C with end-to-end rotation. The immunoprecipitates were washed three times with lysis buffer. The beads were resuspended in 300 μL of 50 mM Tris pH 8.5 containing 5% SDS and protein was eluted by heating at 95°C for 5 minutes.

The eluted protein was proteolytically digested on S-Trap Micro columns (Protifi, C02-micro-10) following the manufacturer's protocol with minor modifications. Briefly, protein was reduced in 5 mM TCEP for 15 minutes at 55°C and then alkylated in 20 mM iodoacetamide for 30 minutes in the dark at room temperature. After adding phosphoric acid to a final concentration of 2.5% (v/v), the protein was diluted in 10 volumes of 100 mM Tris, pH 7.55 in 90% methanol/10% water and bound to the S-Trap column by centrifugation at 4,000xg. The column was washed in the same buffer and then 1 μg of trypsin (Promega, V5113) diluted in 20 μL 50 mM ammonium bicarbonate, pH 8 was applied. After overnight digestion at 37°C, peptides were eluted in 40 μL ammonium bicarbonate pH 8, followed by 40 μL 0.2% formic acid in water, and finally 40 μL 50% acetonitrile in water. The pooled eluate was dried under reduced pressure using a SpeedVac. Dried peptides were resuspended in 950 μL of 85% acetonitrile in water and phosphoenrichment was performed using Fe-NTA IMAC beads (Cell Signaling, 20432S) following the manufacturer's protocol, except a secondary trypsin digestion was not performed. The phosphoenriched and the phosphodepleted fractions were collected and dried using a SpeedVac. Dried phosphoenriched peptides were resuspended in 25 μL 0.1% formic acid in water prior to analysis by LC-MS/MS.

Mass spectrometry

LC-MS/MS method for untargeted peptide detection.—Phosphoenriched peptides were analyzed by LC-MS/MS using a Vanquish Flex LC (ThermoFisher Scientific) directly interfaced to a Q Exactive mass spectrometer (ThermoFisher Scientific). Reconstituted peptides (10 μL) were separated by reversed-phase high performance LC on a 2.1 x 100 mm Acclaim RSLC C18 column (2.2 μm particle size, 120 Å pore size, ThermoFisher Scientific, 068982) at a flow rate of 0.3 mL/min using a linear gradient. For MITF-A samples, the gradient ran from 5–35% mobile phase B (0.1% formic acid in acetonitrile) over 20 minutes, where mobile phase A was 0.1% formic acid in water. For TFE3 samples, an extended gradient of 5–45% mobile phase B over 27 minutes was used. Positive mode electrospray ionization with a HESI-II probe was achieved with a sheath gas flow rate of 35 arbitrary units, auxiliary gas flow rate of 4 arbitrary units, capillary temperature of 320°C, and spray voltage of 3.0 kV. MS analysis was carried out in the Top 5 data dependent acquisition mode. Full MS scans were acquired at a resolution of 70,000 (FWHM) with an automatic gain control target of 1×10^6, m/z scan range of 350–1800, and maximum ion accumulation time of 200 ms. Precursor ions with charges 2–7 and a minimum intensity threshold of 1×10^4 were selected with a quadrupole isolation window of 2.0 m/z for HCD fragmentation with a normalized collision energy (NCE) of 27. MS/MS scans at a resolution of 17,500 were acquired with an ACG target of 1×10^5, a maximum ion accumulation time of 500

ms, and a fixed first mass of 120m/z. Dynamic exclusion was enabled with a duration of 6 seconds.

LC-MS/MS method for targeted peptide detection.—For targeted detection of phosphopeptides, LC-MS/MS was carried out with the same LC gradient and MS source parameters described above. The m/z of the phosphopeptide precursor ions identified in the untargeted runs targeted for selective fragmentation by product reaction monitoring using an NCE of 22.

Dual luciferase assay

TFE3 and MITF double KO HEK-293T cells were generated to stably express the dual luciferase reporter system using lentivirus. To assess TFE3 activity, a 4xCLEAR-*ff*Luciferase PGK-*ren*Luciferase reporter was used, while a 3xM-box-*ff*Luciferase PGK-*ren*Luciferase reporter was used to assess the activity of MITF-A. The PGK-*ren*Luciferase serves as an internal control. In the TFE3/MITF double KO cells stably expressing these luciferase reporters, TFE3 or MITF-A wild type or mutant constructs expressed under the EF1α promoter were complemented by stable integration using lentivirus to achieve roughly similar levels of transduction. Transduction was carried out in biological triplicate for each condition. Two days following transduction, positive cells were selected for using puromycin (2 μg/ml) and the luciferase levels were determined following two days of selection. To obtain the ratio of *ff*Luciferase/*ren*Luciferase, a dual luciferase reporter assay was employed (Promega, E1910). Briefly, selected cells were rinsed once with PBS and lysed with 500 μL of passive lysis buffer (PLB) by gentle rocking for 15 minutes at room temperature. Once lysed, 10 μL of lysate was transferred to the bottom of an opaque 96-well plate. For each of the three biological replicates, three technical replicates were performed. Then, 100 μL of LARII solution was added directly to the bottom of the 96-well plate, homogenized briefly by pipetting, and the *ff*Luciferase levels were determined by measuring luminescence on a plate-reader. The control *ren*Luciferase levels were determined by adding 100 μL of Stop&Glo reagent, homogenized briefly by pipetting, and luminescence measured.

RNA extraction, cDNA generation, and qPCR

RNA was isolated from cells in biological replicates using the RNeasy Plus Mini Kit (Qiagen, 74134) following the manufacturer instructions. Using freshly extracted RNA, cDNA was generated using 250 ng of RNA following the general iScript cDNA Synthesis Kit (BioRad, 1708891) instructions for a 20 μL reaction. qPCR reactions were then performed with the Platinum SYBR Green qPCR Supermix-UDG (Thermo Fisher Scientific, 11733038) and 2 μL of cDNA. A Quantstudio 6 Pro was used to run the qPCR reactions. The following pre-mixed, pre-designed qPCR assay primers obtained from IDT were used:

TFE3: CTCTCATCCCTAAGTCCAGTGA

TGCTCCTTCTGCAGCTTG

MITF: GATTGTCCTTTTTCTGCCTCTC

CTCACCATCAGCAACTCCTG

β-TrCP2: TGCAGTATGATGAGCGTGTC

GGTGGATCAATGTGTTAAGAACTTC

Actin: ACAGAGCCTCGCCTTTG

CCTTGCACATGCCGGAG

HMOX1: TCATGAGGAACTTTCAGAAGGG

TGCGCTCAATCTCCTCCT

PMEL: AGCTTATCATGCCTGGTCAAG

GAAGTCTTGCTTCATAAGTCTGC

Live cell imaging

HEK-293T cells were seeded onto 35 mm glass bottom dishes (Ibidi, 81218–200) that were pre-coated with poly-L-lysine and infected with lentivirus to stably expresses GFP-TFE3 fusion constructs. Three days after transduction, the cells were treated with 5 μg/mL of Hoechst 33342 DNA stain for 1 hour at 37°C (Thermo Fisher Scientific, H3570). Cells were then rinsed twice with PBS and imaged live using a widefield fluorescent microscope and images between mutants were taken without changing laser intensity or exposure time to ensure any changes in fluorescence intensity were rigorously and faithfully captured.

QUANTIFICATION AND STATISTICAL ANALYSIS

Analysis of GPS ORFeome screen

Deconvolution of the pooled screen was achieved by Illumina sequencing. Genomic DNA was extracted from the cells sorted into each stability bin (Qiagen, Gentra Puregene Core Kit, 158767), and the barcodes at the 3' end of each ORF were amplified by PCR (NEB, Q5 Hot Start High-Fidelity DNA Polymerase, M0493L). Following a second round of PCR to add the Illumina P5 and P7 adaptor sequences, samples were pooled evenly and sequenced on a NextSeq 500 instrument. Barcodes were extracted from the resulting sequence reads using Cutadapt and mapped to a custom index using Bowtie 2 to quantify the abundance of each ORF in each stability bin. After a correction for sequencing depth, a protein stability index (PSI) metric between 1 (maximally unstable) and 6 (maximally stable) was calculated for each barcoded ORF using the formula: $\text{PSI} = \sum_{i=1}^{6} Ri * i$, where i=the number of the stability bin and Ri = proportion of Illumina reads present in the given bin i. The change in protein stability between MLN4924 and DMSO is denoted as the difference in PSI (ΔPSI).

Analysis of CRISPR-Cas9 screens

Enrichment of sgRNAs within the 95th percentile relative to the input was achieved by Illumina sequencing. Genomic DNA was extracted from the sorted and input cells (Gentra Puregene Core Kit, Qiagen), and the sgRNAs were amplified by PCR (Q5 Hot Start High-Fidelity DNA Polymerase, NEB). Following a second round of PCR to add the Illumina

P5 and P7 adaptor sequences, samples were pooled in the correct ratio and sequenced on a NextSeq 500 instrument. sgRNAs were extracted from the resulting sequence reads using Cutadapt and mapped to the reference library using Bowtie 2 to quantify the abundance of each sgRNA. Enrichment of sgRNAs relative to the input population was determined using MAGeCK. The MAGeCK score was calculated based on the negative log10 of the "pos|score" value generated by MAGeCK.

Analysis of mass spectrometry data

To identify peptides originating from TFE3 or MITF-A, a FASTA protein database consisting of the Human UniProt SwissProt proteome (downloaded on August 6, 2021) and the sequence of tagged TFE3 or MITF-A was generated. The raw MS data were searched against this database using PEAKS X+ software. Semispecific tryptic peptides with a maximum of three missed cleavages were considered. Carbamidomethylation on Cys was set as a fixed modification. Oxidation of Met and phosphorylation of Ser, Thr, and Tyr were allowed as variable modifications, with a maximum of three variable modifications per peptide. The allowed mass tolerances were 10 ppm for precursor ions and 0.04 Da for product ions. Peptide hits were filtered to a false discovery rate of 1% using the PEAKS decoy-fusion approach.

Analysis of dual luciferase assay and qPCR data

Luciferase data was analyzed using an ordinary one-way ANOVA followed by Tukey's multiple comparisons test where **** represents a P-value 0.0001 and ns represents not passing statistical significance (P > 0.05).

Changes in mRNA levels were determined by subtracting the Cq values obtained during the qPCR between the gene of interest and actin, the internal control (Cq). Values were normalized to the indicated control condition by subtracting the Cq values by the average Cq value of the indicated control condition to obtain the Cq. Plotted are the 2^(– Cq) values from biological replicates and the following statistical tests were performed for the indicated experiment to determine significance.

qPCR (Figure S1B) was analyzed using a two-way ANOVA followed by Šídák's multiple comparisons test where ** represents a P-value 0.005 and ns represents not passing statistical significance (P > 0.05).

qPCR (Figure S1H) was analyzed using a two-way ANOVA followed by Tukey's multiple comparisons test where **** represents a P-value 0.0001, *** a P-value 0.0005, ** a P-value 0.005, * a P-value 0.05, and ns represents not passing statistical significance (P > 0.05).

qPCR (Figure S5E) was analyzed using multiple T-tests followed by a Bonferroni correction where **** represents a P-value 0.00005, *** a P-value 0.0005, ** a P-value 0.005, * a P-value 0.05, and ns represents not passing statistical significance (P > 0.05).

Supplementary Material

Refer to Web version on PubMed Central for supplementary material.

Acknowledgments

REFERENCES

1. Popovic D, Vucic D, and Dikic I (2014). Ubiquitination in disease pathogenesis and treatment. Nat Med 20, 1242–1253. 10.1038/nm.3739. [PubMed: 25375928]

2. Ravid T, and Hochstrasser M (2008). Diversity of degradation signals in the ubiquitin-proteasome system. Nat Rev Mol Cell Biol 9, 679–690. 10.1038/nrm2468. [PubMed: 18698327]

3. Varshavsky A (2019). N-degron and C-degron pathways of protein degradation. Proc Natl Acad Sci U S A 116, 358–366. 10.1073/pnas.1816596116. [PubMed: 30622213]

4. Kaelin WG Jr., and Ratcliffe PJ (2008). Oxygen sensing by metazoans: the central role of the HIF hydroxylase pathway. Mol Cell 30, 393–402. 10.1016/j.molcel.2008.04.009. [PubMed: 18498744]

5. Motohashi H, and Yamamoto M (2004). Nrf2-Keap1 defines a physiologically important stress response mechanism. Trends Mol Med 10, 549–557. 10.1016/j.molmed.2004.09.003. [PubMed: 15519281]

6. Welcker M, Orian A, Jin J, Grim JE, Harper JW, Eisenman RN, and Clurman BE (2004). The Fbw7 tumor suppressor regulates glycogen synthase kinase 3 phosphorylation-dependent c-Myc protein degradation. Proc Natl Acad Sci U S A 101, 9085–9090. 10.1073/pnas.0402770101. [PubMed: 15150404]

7. Hemesath TJ, Steingrimsson E, McGill G, Hansen MJ, Vaught J, Hodgkinson CA, Arnheiter H, Copeland NG, Jenkins NA, and Fisher DE (1994). microphthalmia, a critical factor in melanocyte development, defines a discrete transcription factor family. Genes Dev 8, 2770–2780. 10.1101/gad.8.22.2770. [PubMed: 7958932]

8. La Spina M, Contreras PS, Rissone A, Meena NK, Jeong E, and Martina JA (2020). MiT/TFE Family of Transcription Factors: An Evolutionary Perspective. Front Cell Dev Biol 8, 609683. 10.3389/fcell.2020.609683. [PubMed: 33490073]

9. Goding CR, and Arnheiter H (2019). MITF-the first 25 years. Genes Dev 33, 983–1007. 10.1101/gad.324657.119. [PubMed: 31123060]

10. Kawakami A, and Fisher DE (2017). The master role of microphthalmia-associated transcription factor in melanocyte and melanoma biology. Lab Invest 97, 649–656. 10.1038/labinvest.2017.9. [PubMed: 28263292]

11. Sardiello M, Palmieri M, di Ronza A, Medina DL, Valenza M, Gennarino VA, Di Malta C, Donaudy F, Embrione V, Polishchuk RS, et al. (2009). A gene network regulating lysosomal biogenesis and function. Science 325, 473–477. 10.1126/science.1174447. [PubMed: 19556463]

12. Settembre C, Di Malta C, Polito VA, Garcia Arencibia M, Vetrini F, Erdin S, Erdin SU, Huynh T, Medina D, Colella P, et al. (2011). TFEB links autophagy to lysosomal biogenesis. Science 332, 1429–1433. 10.1126/science.1204592. [PubMed: 21617040]

13. Martina JA, Diab HI, Lishu L, Jeong AL, Patange S, Raben N, and Puertollano R (2014). The nutrient-responsive transcription factor TFE3 promotes autophagy, lysosomal biogenesis, and clearance of cellular debris. Sci Signal 7, ra9. 10.1126/scisignal.2004754. [PubMed: 24448649]

14. Villegas F, Lehalle D, Mayer D, Rittirsch M, Stadler MB, Zinner M, Olivieri D, Vabres P, Duplomb-Jego L, De Bont E, et al. (2019). Lysosomal Signaling Licenses Embryonic Stem Cell Differentiation via Inactivation of Tfe3. Cell Stem Cell 24, 257–270 e258. 10.1016/j.stem.2018.11.021. [PubMed: 30595499]

15. Lehalle D, Vabres P, Sorlin A, Bierhals T, Avila M, Carmignac V, Chevarin M, Torti E, Abe Y, Bartolomaeus T, et al. (2020). De novo mutations in the X-linked TFE3 gene cause intellectual disability with pigmentary mosaicism and storage disorder-like features. J Med Genet 57, 808–819. 10.1136/jmedgenet-2019-106508. [PubMed: 32409512]

16. Diaz J, Berger S, and Leon E (2020). TFE3-associated neurodevelopmental disorder: A distinct recognizable syndrome. Am J Med Genet A 182, 584–590. 10.1002/ajmg.a.61437. [PubMed: 31833172]

17. Kauffman EC, Ricketts CJ, Rais-Bahrami S, Yang Y, Merino MJ, Bottaro DP, Srinivasan R, and Linehan WM (2014). Molecular genetics and cellular features of TFE3 and TFEB fusion kidney cancers. Nat Rev Urol 11, 465–475. 10.1038/nrurol.2014.162. [PubMed: 25048860]

18. Roczniak-Ferguson A, Petit CS, Froehlich F, Qian S, Ky J, Angarola B, Walther TC, and Ferguson SM (2012). The transcription factor TFEB links mTORC1 signaling to transcriptional control of lysosome homeostasis. Sci Signal 5, ra42. 10.1126/scisignal.2002790. [PubMed: 22692423]

19. Settembre C, Zoncu R, Medina DL, Vetrini F, Erdin S, Erdin S, Huynh T, Ferron M, Karsenty G, Vellard MC, et al. (2012). A lysosome-to-nucleus signalling mechanism senses and regulates the lysosome via mTOR and TFEB. EMBO J 31, 1095–1108. 10.1038/emboj.2012.32. [PubMed: 22343943]

20. Martina JA, and Puertollano R (2013). Rag GTPases mediate amino acid-dependent recruitment of TFEB and MITF to lysosomes. J Cell Biol 200, 475–491. 10.1083/jcb.201209135. [PubMed: 23401004]

21. Martina JA, Chen Y, Gucek M, and Puertollano R (2012). MTORC1 functions as a transcriptional regulator of autophagy by preventing nuclear transport of TFEB. Autophagy 8, 903–914. 10.4161/auto.19653. [PubMed: 22576015]

22. Saxton RA, and Sabatini DM (2017). mTOR Signaling in Growth, Metabolism, and Disease. Cell 168, 960–976. 10.1016/j.cell.2017.02.004. [PubMed: 28283069]

23. Liu GY, and Sabatini DM (2020). mTOR at the nexus of nutrition, growth, ageing and disease. Nat Rev Mol Cell Biol 21, 183–203. 10.1038/s41580-019-0199-y. [PubMed: 31937935]

24. Puertollano R, Ferguson SM, Brugarolas J, and Ballabio A (2018). The complex relationship between TFEB transcription factor phosphorylation and subcellular localization. EMBO J 37. 10.15252/embj.201798804.

25. Yen HC, Xu Q, Chou DM, Zhao Z, and Elledge SJ (2008). Global protein stability profiling in mammalian cells. Science 322, 918–923. 10.1126/science.1160489. [PubMed: 18988847]

26. Yen HC, and Elledge SJ (2008). Identification of SCF ubiquitin ligase substrates by global protein stability profiling. Science 322, 923–929. 10.1126/science.1160462. [PubMed: 18988848]

27. Koren I, Timms RT, Kula T, Xu Q, Li MZ, and Elledge SJ (2018). The Eukaryotic Proteome Is Shaped by E3 Ubiquitin Ligases Targeting C-Terminal Degrons. Cell 173, 1622–1635 e1614. 10.1016/j.cell.2018.04.028. [PubMed: 29779948]

28. Harper JW, and Schulman BA (2021). Cullin-RING Ubiquitin Ligase Regulatory Circuits: A Quarter Century Beyond the F-Box Hypothesis. Annu Rev Biochem 90, 403–429. 10.1146/annurev-biochem-090120-013613. [PubMed: 33823649]

29. Lambert SA, Jolma A, Campitelli LF, Das PK, Yin Y, Albu M, Chen X, Taipale J, Hughes TR, and Weirauch MT (2018). The Human Transcription Factors. Cell 172, 650–665. 10.1016/j.cell.2018.01.029. [PubMed: 29425488]

30. Skowyra D, Craig KL, Tyers M, Elledge SJ, and Harper JW (1997). F-box proteins are receptors that recruit phosphorylated substrates to the SCF ubiquitin-ligase complex. Cell 91, 209–219. 10.1016/s0092-8674(00)80403-1. [PubMed: 9346238]

31. Bi Y, Cui D, Xiong X, and Zhao Y (2021). The characteristics and roles of beta-TrCP1/2 in carcinogenesis. FEBS J 288, 3351–3374. 10.1111/febs.15585. [PubMed: 33021036]

32. Wu G, Xu G, Schulman BA, Jeffrey PD, Harper JW, and Pavletich NP (2003). Structure of a beta-TrCP1-Skp1-beta-catenin complex: destruction motif binding and lysine specificity of the

SCF(beta-TrCP1) ubiquitin ligase. Mol Cell 11, 1445–1456. 10.1016/s1097-2765(03)00234-x. [PubMed: 12820959]

33. Skaar JR, Pagan JK, and Pagano M (2013). Mechanisms and function of substrate recruitment by F-box proteins. Nat Rev Mol Cell Biol 14, 369–381. 10.1038/nrm3582. [PubMed: 23657496]

34. Park HS, Hohn MJ, Umehara T, Guo LT, Osborne EM, Benner J, Noren CJ, Rinehart J, and Soll D (2011). Expanding the genetic code of Escherichia coli with phosphoserine. Science 333, 1151–1154. 10.1126/science.1207203. [PubMed: 21868676]

35. Sancak Y, Peterson TR, Shaul YD, Lindquist RA, Thoreen CC, Bar-Peled L, and Sabatini DM (2008). The Rag GTPases bind raptor and mediate amino acid signaling to mTORC1. Science 320, 1496–1501. 10.1126/science.1157535. [PubMed: 18497260]

36. Kim E, Goraksha-Hicks P, Li L, Neufeld TP, and Guan KL (2008). Regulation of TORC1 by Rag GTPases in nutrient response. Nat Cell Biol 10, 935–945. 10.1038/ncb1753. [PubMed: 18604198]

37. Sancak Y, Bar-Peled L, Zoncu R, Markhard AL, Nada S, and Sabatini DM (2010). Ragulator-Rag complex targets mTORC1 to the lysosomal surface and is necessary for its activation by amino acids. Cell 141, 290–303. 10.1016/j.cell.2010.02.024. [PubMed: 20381137]

38. Stocker H, Radimerski T, Schindelholz B, Wittwer F, Belawat P, Daram P, Breuer S, Thomas G, and Hafen E (2003). Rheb is an essential regulator of S6K in controlling cell growth in Drosophila. Nat Cell Biol 5, 559–565. 10.1038/ncb995. [PubMed: 12766775]

39. Saucedo LJ, Gao X, Chiarelli DA, Li L, Pan D, and Edgar BA (2003). Rheb promotes cell growth as a component of the insulin/TOR signalling network. Nat Cell Biol 5, 566–571. 10.1038/ncb996. [PubMed: 12766776]

40. Rogala KB, Gu X, Kedir JF, Abu-Remaileh M, Bianchi LF, Bottino AMS, Dueholm R, Niehaus A, Overwijn D, Fils AP, et al. (2019). Structural basis for the docking of mTORC1 on the lysosomal surface. Science 366, 468–475. 10.1126/science.aay0166. [PubMed: 31601708]

41. Bronisz A, Sharma SM, Hu R, Godlewski J, Tzivion G, Mansky KC, and Ostrowski MC (2006). Microphthalmia-associated transcription factor interactions with 14-3-3 modulate differentiation of committed myeloid precursors. Mol Biol Cell 17, 3897–3906. 10.1091/mbc.e06-05-0470. [PubMed: 16822840]

42. Hu Z, Li H, Jiang H, Ren Y, Yu X, Qiu J, Stablewski AB, Zhang B, Buck MJ, and Feng J (2020). Transient inhibition of mTOR in human pluripotent stem cells enables robust formation of mouse-human chimeric embryos. Sci Adv 6, eaaz0298. 10.1126/sciadv.aaz0298. [PubMed: 32426495]

43. Funasaki S, Mehanna S, Ma W, Nishizawa H, Kamikubo Y, Sugiyama H, Ikeda S, Motoshima T, Hasumi H, Linehan WM, et al. (2022). Targeting chemoresistance in Xp11.2 translocation renal cell carcinoma using a novel polyamide-chlorambucil conjugate. Cancer Sci 113, 2352–2367. 10.1111/cas.15364. [PubMed: 35396773]

44. Ladanyi M, Lui MY, Antonescu CR, Krause-Boehm A, Meindl A, Argani P, Healey JH, Ueda T, Yoshikawa H, Meloni-Ehrig A, et al. (2001). The der(17)t(X;17)(p11;q25) of human alveolar soft part sarcoma fuses the TFE3 transcription factor gene to ASPL, a novel gene at 17q25. Oncogene 20, 48–57. 10.1038/sj.onc.1204074. [PubMed: 11244503]

45. Aulmann S, Longerich T, Schirmacher P, Mechtersheimer G, and Penzel R (2007). Detection of the ASPSCR1-TFE3 gene fusion in paraffin-embedded alveolar soft part sarcomas. Histopathology 50, 881–886. 10.1111/j.1365-2559.2007.02693.x. [PubMed: 17543078]

46. Argani P, Lui MY, Couturier J, Bouvier R, Fournet JC, and Ladanyi M (2003). A novel CLTC-TFE3 gene fusion in pediatric renal adenocarcinoma with t(X;17)(p11.2;q23). Oncogene 22, 5374–5378. 10.1038/sj.onc.1206686. [PubMed: 12917640]

47. Agaram NP, Sung YS, Zhang L, Chen CL, Chen HW, Singer S, Dickson MA, Berger MF, and Antonescu CR (2015). Dichotomy of Genetic Abnormalities in PEComas With Therapeutic Implications. Am J Surg Pathol 39, 813–825. 10.1097/PAS.0000000000000389. [PubMed: 25651471]

48. Fukuda H, Kato I, Furuya M, Tanaka R, Takagi T, Kondo T, and Nagashima Y (2019). A novel partner of TFE3 in the Xp11 translocation renal cell carcinoma: clinicopathological analyses and detection of EWSR1-TFE3 fusion. Virchows Arch 474, 389–393. 10.1007/s00428-018-2509-8. [PubMed: 30552521]

49. Lang XP, Pan J, Yang CX, Chen P, Shi CC, Hong Y, Wang J, and Xiao S (2020). A renal cell carcinoma with EWSR1-TFE3 fusion gene. Genes Chromosomes Cancer 59, 325–329. 10.1002/gcc.22830. [PubMed: 31774608]

50. Wang XT, Xia QY, Ye SB, Wang X, Li R, Fang R, Shi SS, Zhang RS, Tan X, Chen JY, et al. (2018). RNA sequencing of Xp11 translocation-associated cancers reveals novel gene fusions and distinctive clinicopathologic correlations. Mod Pathol 31, 1346–1360. 10.1038/s41379-018-0051-5. [PubMed: 29713041]

51. Malouf GG, Su X, Yao H, Gao J, Xiong L, He Q, Comperat E, Couturier J, Molinie V, Escudier B, et al. (2014). Next-generation sequencing of translocation renal cell carcinoma reveals novel RNA splicing partners and frequent mutations of chromatin-remodeling genes. Clin Cancer Res 20, 4129–4140. 10.1158/1078-0432.CCR-13-3036. [PubMed: 24899691]

52. Clark J, Lu YJ, Sidhar SK, Parker C, Gill S, Smedley D, Hamoudi R, Linehan WM, Shipley J, and Cooper CS (1997). Fusion of splicing factor genes PSF and NonO (p54nrb) to the TFE3 gene in papillary renal cell carcinoma. Oncogene 15, 2233–2239. 10.1038/sj.onc.1201394. [PubMed: 9393982]

53. Xia QY, Wang Z, Chen N, Gan HL, Teng XD, Shi SS, Wang X, Wei X, Ye SB, Li R, et al. (2017). Xp11.2 translocation renal cell carcinoma with NONO-TFE3 gene fusion: morphology, prognosis, and potential pitfall in detecting TFE3 gene rearrangement. Mod Pathol 30, 416–426. 10.1038/modpathol.2016.204. [PubMed: 27934879]

54. Huang W, Goldfischer M, Babayeva S, Mao Y, Volyanskyy K, Dimitrova N, Fallon JT, and Zhong M (2015). Identification of a novel PARP14-TFE3 gene fusion from 10-year-old FFPE tissue by RNA-seq. Genes Chromosomes Cancer 54, 500–505. 10.1002/gcc.22261. [PubMed: 26032162]

55. Suurmeijer AJH, Song W, Sung YS, Zhang L, Swanson D, Fletcher CDM, Dickson BC, and Antonescu CR (2019). Novel recurrent PHF1-TFE3 fusions in ossifying fibromyxoid tumors. Genes Chromosomes Cancer 58, 643–649. 10.1002/gcc.22755. [PubMed: 30920708]

56. Panagopoulos I, Gorunova L, Lund-Iversen M, Bassarova A, and Heim S (2019). Fusion of the Genes PHF1 and TFE3 in Malignant Chondroid Syringoma. Cancer Genomics Proteomics 16, 345–351. 10.21873/cgp.20139. [PubMed: 31467228]

57. Argani P, Antonescu CR, Couturier J, Fournet JC, Sciot R, Debiec-Rychter M, Hutchinson B, Reuter VE, Boccon-Gibod L, Timmons C, et al. (2002). PRCC-TFE3 renal carcinomas: morphologic, immunohistochemical, ultrastructural, and molecular analysis of an entity associated with the t(X;1)(p11.2;q21). Am J Surg Pathol 26, 1553–1566. 10.1097/00000478-200212000-00003. [PubMed: 12459622]

58. Weterman MA, Wilbrink M, and Geurts van Kessel A (1996). Fusion of the transcription factor TFE3 gene to a novel gene, PRCC, in t(X;1)(p11;q21)-positive papillary renal cell carcinomas. Proc Natl Acad Sci U S A 93, 15294–15298. 10.1073/pnas.93.26.15294. [PubMed: 8986805]

59. Sidhar SK, Clark J, Gill S, Hamoudi R, Crew AJ, Gwilliam R, Ross M, Linehan WM, Birdsall S, Shipley J, and Cooper CS (1996). The t(X;1)(p11.2;q21.2) translocation in papillary renal cell carcinoma fuses a novel gene PRCC to the TFE3 transcription factor gene. Hum Mol Genet 5, 1333–1338. 10.1093/hmg/5.9.1333. [PubMed: 8872474]

60. Just PA, Letourneur F, Pouliquen C, Dome F, Audebourg A, Biquet P, Vidaud M, Terris B, Sibony M, and Pasmant E (2016). Identification by FFPE RNA-Seq of a new recurrent inversion leading to RBM10-TFE3 fusion in renal cell carcinoma with subtle TFE3 break-apart FISH pattern. Genes Chromosomes Cancer 55, 541–548. 10.1002/gcc.22356. [PubMed: 26998913]

61. Argani P, Zhang L, Sung YS, White MJ, Miller K, Hopkins M, Small D, Pratilas CA, Swanson D, Dickson B, and Antonescu CR (2019). A novel RBMX-TFE3 gene fusion in a highly aggressive pediatric renal perivascular epithelioid cell tumor. Genes Chromosomes Cancer. 10.1002/gcc.22801.

62. Rao Q, Shen Q, Xia QY, Wang ZY, Liu B, Shi SS, Shi QL, Yin HL, Wu B, Ye SB, et al. (2015). PSF/SFPQ is a very common gene fusion partner in TFE3 rearrangement-associated perivascular epithelioid cell tumors (PEComas) and melanotic Xp11 translocation renal cancers: clinicopathologic, immunohistochemical, and molecular characteristics suggesting classification as a distinct entity. Am J Surg Pathol 39, 1181–1196. 10.1097/PAS.0000000000000502. [PubMed: 26274027]

63. Antonescu CR, Le Loarer F, Mosquera JM, Sboner A, Zhang L, Chen CL, Chen HW, Pathan N, Krausz T, Dickson BC, et al. (2013). Novel YAP1-TFE3 fusion defines a distinct subset of epithelioid hemangioendothelioma. Genes Chromosomes Cancer 52, 775–784. 10.1002/gcc.22073. [PubMed: 23737213]

64. Xia QY, Wang XT, Ye SB, Wang X, Li R, Shi SS, Fang R, Zhang RS, Ma HH, Lu ZF, et al. (2018). Novel gene fusion of PRCC-MITF defines a new member of MiT family translocation renal cell carcinoma: clinicopathological analysis and detection of the gene fusion by RNA sequencing and FISH. Histopathology 72, 786–794. 10.1111/his.13439. [PubMed: 29148086]

65. Jumper J, Evans R, Pritzel A, Green T, Figurnov M, Ronneberger O, Tunyasuvunakool K, Bates R, Zidek A, Potapenko A, et al. (2021). Highly accurate protein structure prediction with AlphaFold. Nature 596, 583–589. 10.1038/s41586-021-03819-2. [PubMed: 34265844]

66. Mirdita M, Schutze K, Moriwaki Y, Heo L, Ovchinnikov S, and Steinegger M (2022). ColabFold: making protein folding accessible to all. Nat Methods 19, 679–682. 10.1038/s41592-022-01488-1. [PubMed: 35637307]

67. Steingrimsson E, Tessarollo L, Pathak B, Hou L, Arnheiter H, Copeland NG, and Jenkins NA (2002). Mitf and Tfe3, two members of the Mitf-Tfe family of bHLH-Zip transcription factors, have important but functionally redundant roles in osteoclast development. Proc Natl Acad Sci U S A 99, 4477–4482. 10.1073/pnas.072071099. [PubMed: 11930005]

68. Bakouny Z, Sadagopan A, Ravi P, Metaferia NY, Li J, AbuHammad S, Tang S, Denize T, Garner ER, Gao X, et al. (2022). Integrative clinical and molecular characterization of translocation renal cell carcinoma. Cell Rep 38, 110190. 10.1016/j.celrep.2021.110190. [PubMed: 34986355]

69. Bastus NC, Boyd LK, Mao X, Stankiewicz E, Kudahetti SC, Oliver RT, Berney DM, and Lu YJ (2010). Androgen-induced TMPRSS2:ERG fusion in nonmalignant prostate epithelial cells. Cancer Res 70, 9544–9548. 10.1158/0008-5472.CAN-10-1638. [PubMed: 20947519]

70. Gosis BS, Wada S, Thorsheim C, Li K, Jung S, Rhoades JH, Yang Y, Brandimarto J, Li L, Uehara K, et al. (2022). Inhibition of nonalcoholic fatty liver disease in mice by selective inhibition of mTORC1. Science 376, eabf8271. 10.1126/science.abf8271. [PubMed: 35420934]

71. Mohler K, Moen J, Rogulina S, and Rinehart J (2021). Principles for Systematic Optimization of an Orthogonal Translation System with Enhanced Biological Tolerance. bioRxiv, 2021.2005.2020.444985 10.1101/2021.05.20.444985.

72. Martin TD, Patel RS, Cook DR, Choi MY, Patil A, Liang AC, Li MZ, Haigis KM, and Elledge SJ (2021). The adaptive immune system is a major driver of selection for tumor suppressor gene inactivation. Science 373, 1327–1335. 10.1126/science.abg5784. [PubMed: 34529489]

73. Oreskovic E, Wheeler EC, Mengwasser KE, Fujimura E, Martin TD, Tothova Z, and Elledge SJ (2022). Genetic analysis of cancer drivers reveals cohesin and CTCF as suppressors of PD-L1. Proc Natl Acad Sci U S A 119. 10.1073/pnas.2120540119.

74. Timms RT, Zhang Z, Rhee DY, Harper JW, Koren I, and Elledge SJ (2019). A glycine-specific N-degron pathway mediates the quality control of protein N-myristoylation. Science 365. 10.1126/science.aaw4912.

75. Doench JG, Fusi N, Sullender M, Hegde M, Vaimberg EW, Donovan KF, Smith I, Tothova Z, Wilen C, Orchard R, et al. (2016). Optimized sgRNA design to maximize activity and minimize off-target effects of CRISPR-Cas9. Nat Biotechnol 34, 184–191. 10.1038/nbt.3437. [PubMed: 26780180]

76. Langmead B, and Salzberg SL (2012). Fast gapped-read alignment with Bowtie 2. Nat Methods 9, 357–359. 10.1038/nmeth.1923. [PubMed: 22388286]

77. Langmead B, Trapnell C, Pop M, and Salzberg SL (2009). Ultrafast and memory-efficient alignment of short DNA sequences to the human genome. Genome Biol 10, R25. 10.1186/gb-2009-10-3-r25. [PubMed: 19261174]

78. Martin M (2011). Cutadapt removes adapter sequences from high-throughput sequencing reads. EMBnet.journal 17, 10–12.

79. Li W, Xu H, Xiao T, Cong L, Love MI, Zhang F, Irizarry RA, Liu JS, Brown M, and Liu XS (2014). MAGeCK enables robust identification of essential genes from genome-scale CRISPR/Cas9 knockout screens. Genome Biol 15, 554. 10.1186/s13059-014-0554-4. [PubMed: 25476604]

80. Varadi M, Anyango S, Deshpande M, Nair S, Natassia C, Yordanova G, Yuan D, Stroe O, Wood G, Laydon A, et al. (2022). AlphaFold Protein Structure Database: massively expanding the structural coverage of protein-sequence space with high-accuracy models. Nucleic Acids Res 50, D439–D444. 10.1093/nar/gkab1061. [PubMed: 34791371]

81. Pettersen EF, Goddard TD, Huang CC, Meng EC, Couch GS, Croll TI, Morris JH, and Ferrin TE (2021). UCSF ChimeraX: Structure visualization for researchers, educators, and developers. Protein Sci 30, 70–82. 10.1002/pro.3943. [PubMed: 32881101]

82. Goddard TD, Huang CC, Meng EC, Pettersen EF, Couch GS, Morris JH, and Ferrin TE (2018). UCSF ChimeraX: Meeting modern challenges in visualization and analysis. Protein Sci 27, 14–25. 10.1002/pro.3235. [PubMed: 28710774]

83. Waterhouse AM, Procter JB, Martin DM, Clamp M, and Barton GJ (2009). Jalview Version 2--a multiple sequence alignment editor and analysis workbench. Bioinformatics 25, 1189–1191. 10.1093/bioinformatics/btp033. [PubMed: 19151095]

84. Qi LS, Larson MH, Gilbert LA, Doudna JA, Weissman JS, Arkin AP, and Lim WA (2013). Repurposing CRISPR as an RNA-guided platform for sequence-specific control of gene expression. Cell 152, 1173–1183. 10.1016/j.cell.2013.02.022. [PubMed: 23452860]

85. Pirman NL, Barber KW, Aerni HR, Ma NJ, Haimovich AD, Rogulina S, Isaacs FJ, and Rinehart J (2015). A flexible codon in genomically recoded Escherichia coli permits programmable protein phosphorylation. Nat Commun 6, 8130. 10.1038/ncomms9130. [PubMed: 26350500]

86. Barber KW, Muir P, Szeligowski RV, Rogulina S, Gerstein M, Sampson JR, Isaacs FJ, and Rinehart J (2018). Encoding human serine phosphopeptides in bacteria for proteome-wide identification of phosphorylation-dependent interactions. Nat Biotechnol 36, 638–644. 10.1038/nbt.4150. [PubMed: 29889213]

87. Barber KW, Miller CJ, Jun JW, Lou HJ, Turk BE, and Rinehart J (2018). Kinase Substrate Profiling Using a Proteome-wide Serine-Oriented Human Peptide Library. Biochemistry 57, 4717–4725. 10.1021/acs.biochem.8b00410. [PubMed: 29920078]

88. Lajoie MJ, Rovner AJ, Goodman DB, Aerni HR, Haimovich AD, Kuznetsov G, Mercer JA, Wang HH, Carr PA, Mosberg JA, et al. (2013). Genomically recoded organisms expand biological functions. Science 342, 357–360. 10.1126/science.1241459. [PubMed: 24136966]

89. Scott DC, Rhee DY, Duda DM, Kelsall IR, Olszewski JL, Paulo JA, de Jong A, Ovaa H, Alpi AF, Harper JW, and Schulman BA (2016). Two Distinct Types of E3 Ligases Work in Unison to Regulate Substrate Ubiquitylation. Cell 166, 1198–1214 e1124. 10.1016/j.cell.2016.07.027. [PubMed: 27565346]

90. Scott DC, Sviderskiy VO, Monda JK, Lydeard JR, Cho SE, Harper JW, and Schulman BA (2014). Structure of a RING E3 trapped in action reveals ligation mechanism for the ubiquitin-like protein NEDD8. Cell 157, 1671–1684. 10.1016/j.cell.2014.04.037. [PubMed: 24949976]

91. Scott DC, and Schulman BA (2019). Dual-color pulse-chase ubiquitination assays to simultaneously monitor substrate priming and extension. Methods Enzymol 618, 29–48. 10.1016/bs.mie.2019.01.004. [PubMed: 30850057]

Highlights

- Phosphorylation of TFE3/MITF at a conserved serine activates a CUL1$^{\beta\text{-TrCP}}$ degron

- Rag GTPases recruit these TFs to the lysosomal surface to promote their destruction

- The degron within TFE3 is recurrently lost in translocation renal cell carcinoma

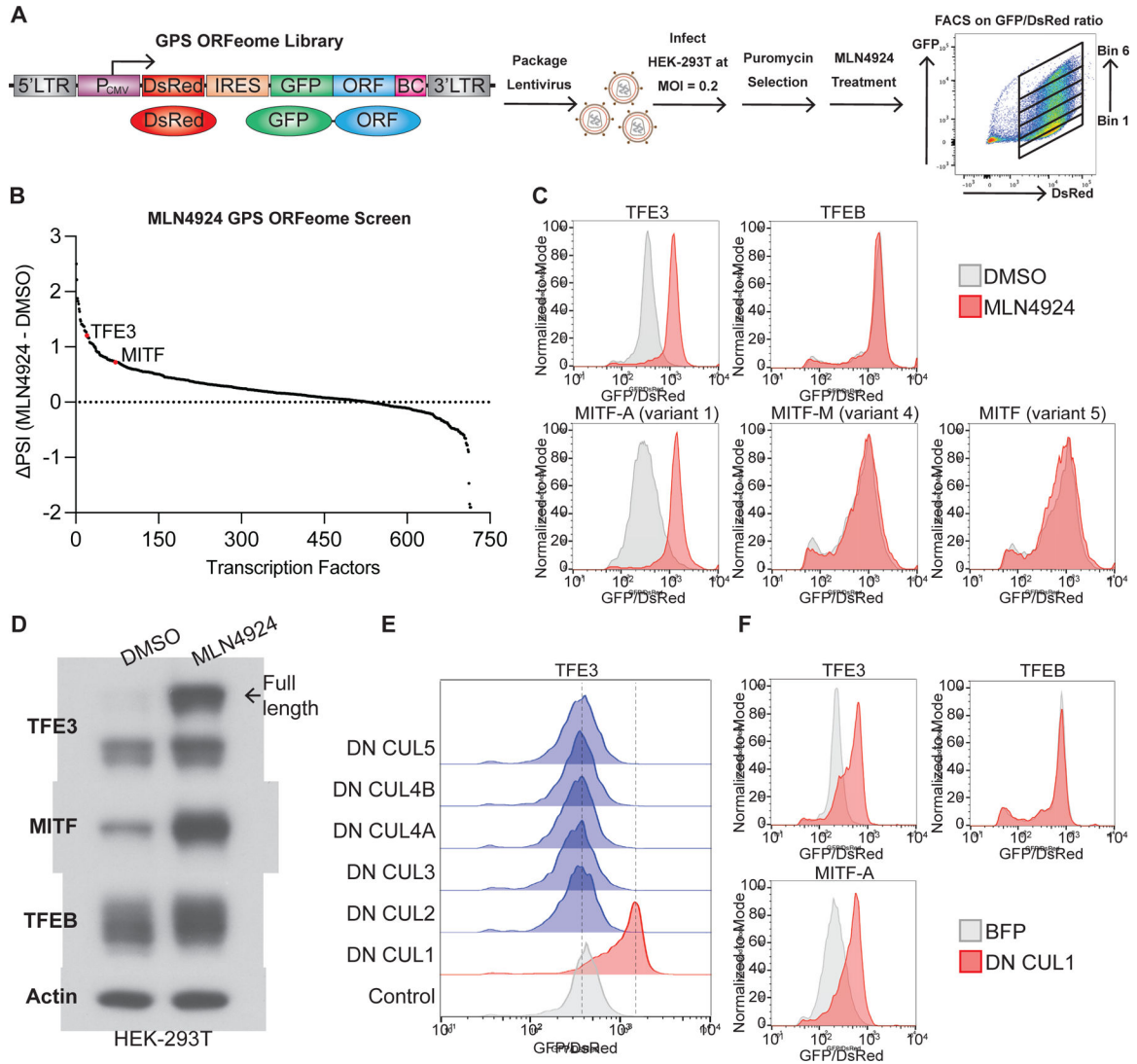- Mutations within the TFE3-RagA interface cause a neurodevelopmental syndrome

Figure 1. GPS ORFeome screen identifies TFE3 and MITF-A as putative Cullin substrates.

(A) Schematic representation of the GPS ORFeome screen −/+ 1 μM MLN4924. An increased ratio of GFP/DsRed signified increased stability of the GFP-ORF fusion protein.

(B) Analysis of GPS ORFeome screen for transcription factors identifies TFE3 and MITF as putative substrates for cullin-RING-ligases. Plotted is the change in the protein stability index (PSI). See also Table S1.

(C) Validation of the GPS ORFeome screen by flow cytometry analysis of GFP/DsRed ratio in HEK-293T cells stably expressing GPS reporters for MiT/TFE family members −/+ 1 μM MLN4924.

(D) Immunoblotting of MiT/TFE family members −/+ 1 μM MLN4924. The upper ~90 kDa species represents the full length TFE3, while the lower ~70 kDa band may be a post-translationally processed or internally translated isoform.

(E) HEK-293T cells stably expressing the GPS TFE3 reporter were transfected with dominant negative (DN) Cullin constructs and analyzed by flow cytometry.

(F) HEK-293T cells stably expressing GPS reporters for MiT/TFE family members were transfected with DN CUL1 and analyzed by flow cytometry. All flow cytometry data is plotted using FlowJo.
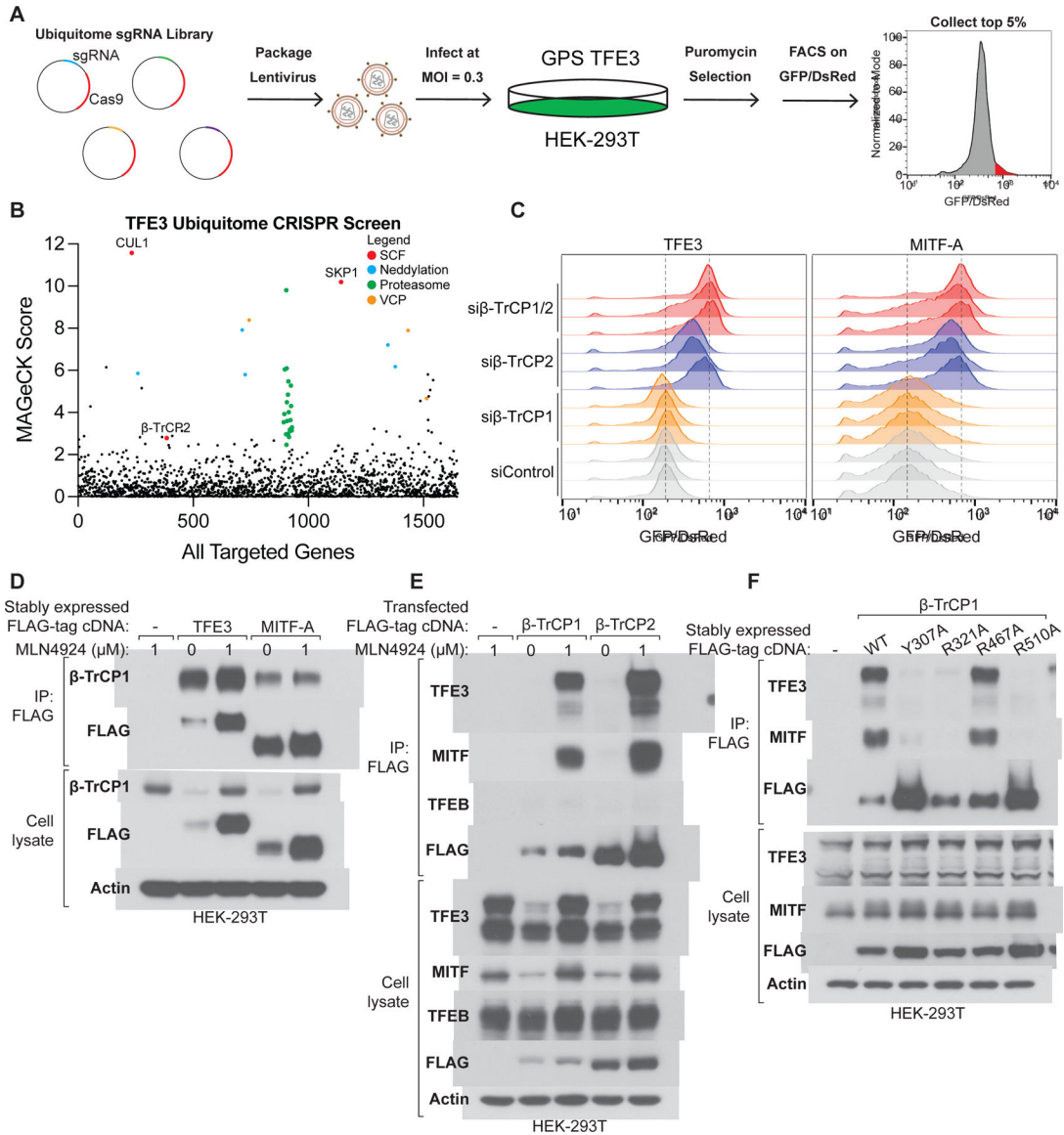
Figure 2. TFE3 and MITF-A are targeted for proteasomal degradation by CUL1$^{\beta\text{-TrCP1/2}}$.

(A) Schematic representation of CRISPR-Cas9 screen performed in HEK-293T cells stably expressing the GPS TFE3 reporter using a curated library of guide RNAs that target genes with known or predicted function related to the ubiquitin-proteasome system (ubiquitome). The top 5% most stable population was collected for enrichment analysis relative to the input population.

(B) Results of the GPS TFE3 screen highlighting the CUL1 complex in red. See also Table S2.

(C) HEK-293T cells stably expressing GPS TFE3 or MITF-A reporters were transfected with three different non-targeting control or siRNAs targeting β-TrCP1/2. Cells were analyzed by flow cytometry 72 hours post-transfection.

(D) Immunoblotting from anti-FLAG immunoprecipitates of stably expressed FLAG-tagged TFE3 or MITF-A –/+ 1 μM MLN4924.

(E) Immunoblotting from anti-FLAG immunoprecipitates of transfected FLAG-tagged β-TrCP1/2 –/+ 1 μM MLN4924.

(F) Immunoblotting from anti-FLAG immunoprecipitates of stably expressed FLAG-tagged β-TrCP1 in the presence of 1 μM MLN4924.
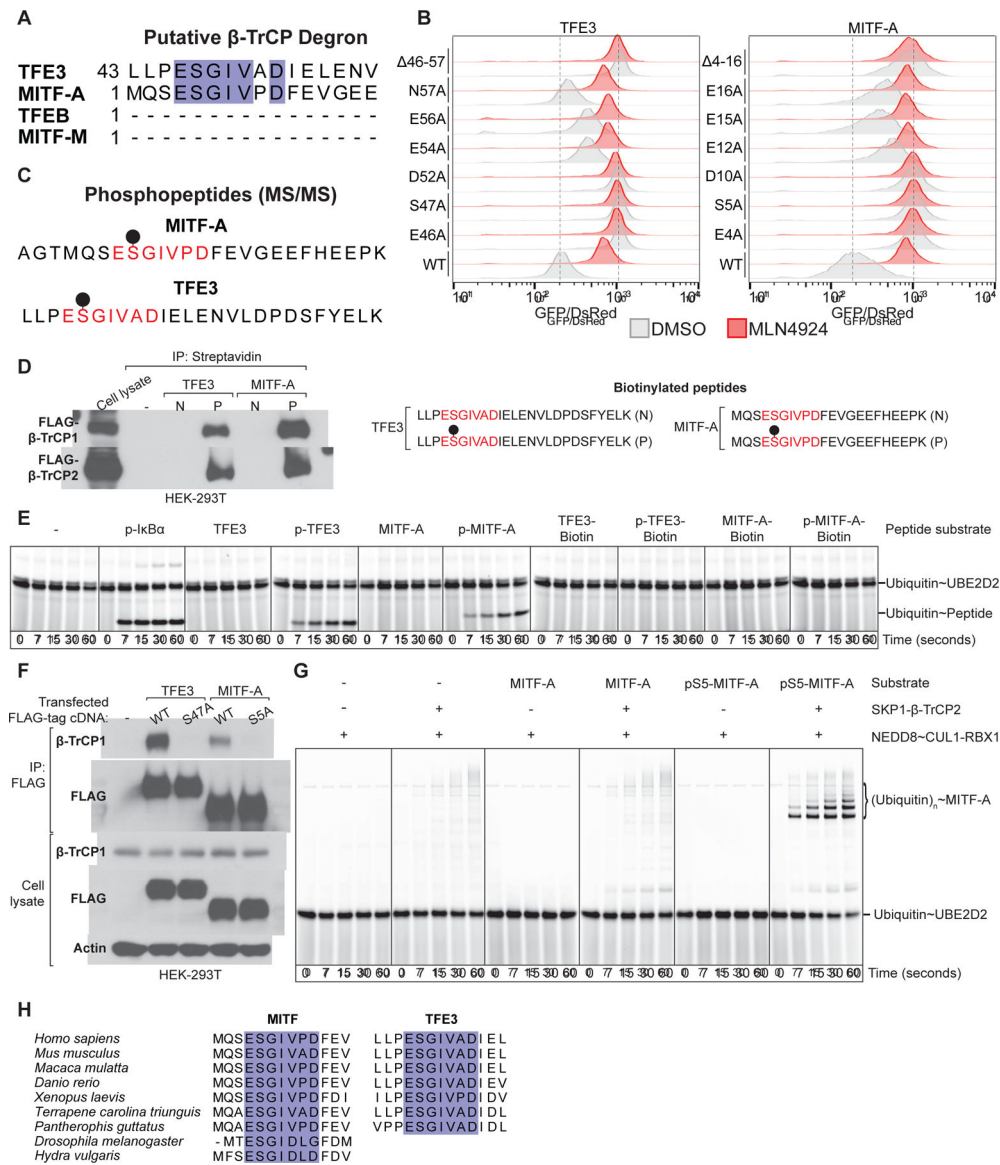
Figure 3. Phosphorylation of a conserved degron within TFE3 and MITF-A is necessary for ubiquitination by CUL1^β-TrCP1/2.

(A) Amino acid sequence alignment of the MiT/TFE family revealed a putative β-TrCP degron motif (ESGIVxD). Figure made using Jalview.

(B) TFE3 and MITF-A were mutagenized within and outside the putative degron. HEK-293T cells stably expressing GPS reporters of these mutants were analyzed by flow cytometry –/+ 1 μM MLN4924.

(C) Phosphopeptides identified by LC-MS/MS following phospho-enrichment of TFE3^S42R and MITF-A tryptic peptides. See also Figure S2, Figure S3, and Table S3.

(D) Immunoblotting from streptavidin enrichment of biotin-labeled synthetic peptides in the native (N) or degron phosphorylated (P) state incubated with transfected FLAG-tagged β-TrCP1/2 cell lysates.

(E) *In vitro* ubiquitination reaction traced using fluorescent ubiquitin. Reconstituted NEDDylated CUL1$^{\beta\text{-TrCP2}}$ was incubated with the indicated native and phosphorylated peptides.

(F) Immunoblotting from anti-FLAG immunoprecipitates of transfected FLAG-tagged TFE3 or MITF-A in the presence of 1 μM MLN4924.

(G) Similar assay as in (E) using the indicated native and degron phosphorylated recombinant full-length MITF-A. See also Figure S4 and Table S4.

(H) Amino acid sequence comparison of TFE3 and MITF from *Hydra vulgaris* to humans. Figure made using Jalview.
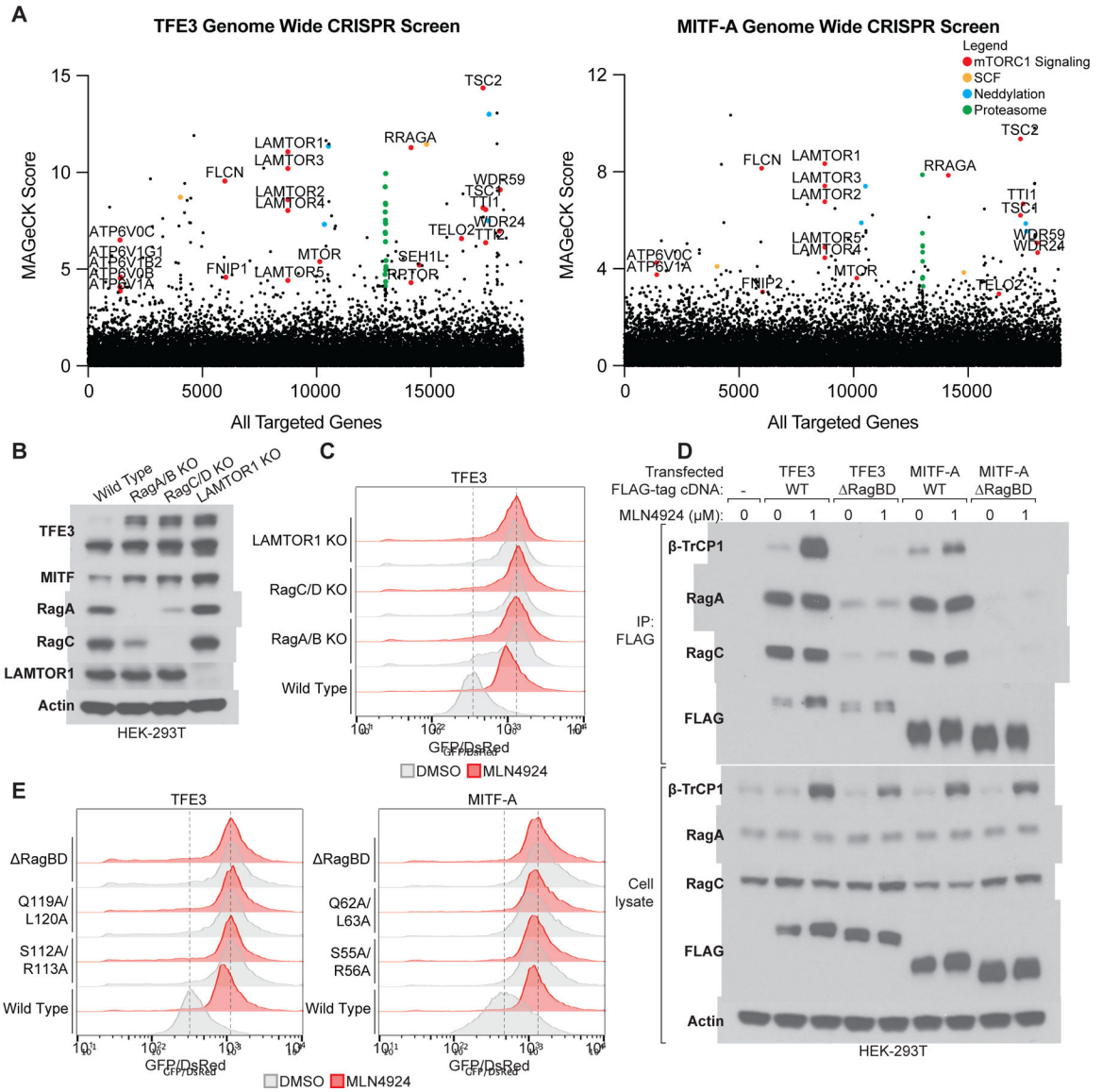
Figure 4. Active Rag GTPases promote CUL1$^{β-TrCP1/2}$-dependent degradation.

(**A**) Results of genome-wide CRISPR-Cas9 screens to identify mutants that result in stabilization of TFE3 and MITF-A, highlighting the Rag GTPases-mTORC1 signaling pathway. See also Table S5.

(**B**) Immunoblotting in wild type, RagA/B, RagC/D, and LAMTOR1 KO HEK-293T.

(**C**) Flow cytometry analysis of wild type**,** RagA/B, RagC/D, and LAMTOR1 KO HEK-293T cells stably expressing the GPS TFE3 reporter −/+ 1 μM MLN4924.

(**D**) Immunoblotting from anti-FLAG immunoprecipitates of transfected FLAG-tagged TFE3 or MITF-A −/+ 1 μM MLN4924. The   RagBD is defined by a deletion of amino acids 112–132 for TFE3 and 55–75 for MITF-A.

(**E**) Flow cytometry analysis of HEK-293T cells stably expressing wild type or mutant TFE3 and MITF-A within the Rag binding domain (RagBD) −/+ 1 μM MLN4924.
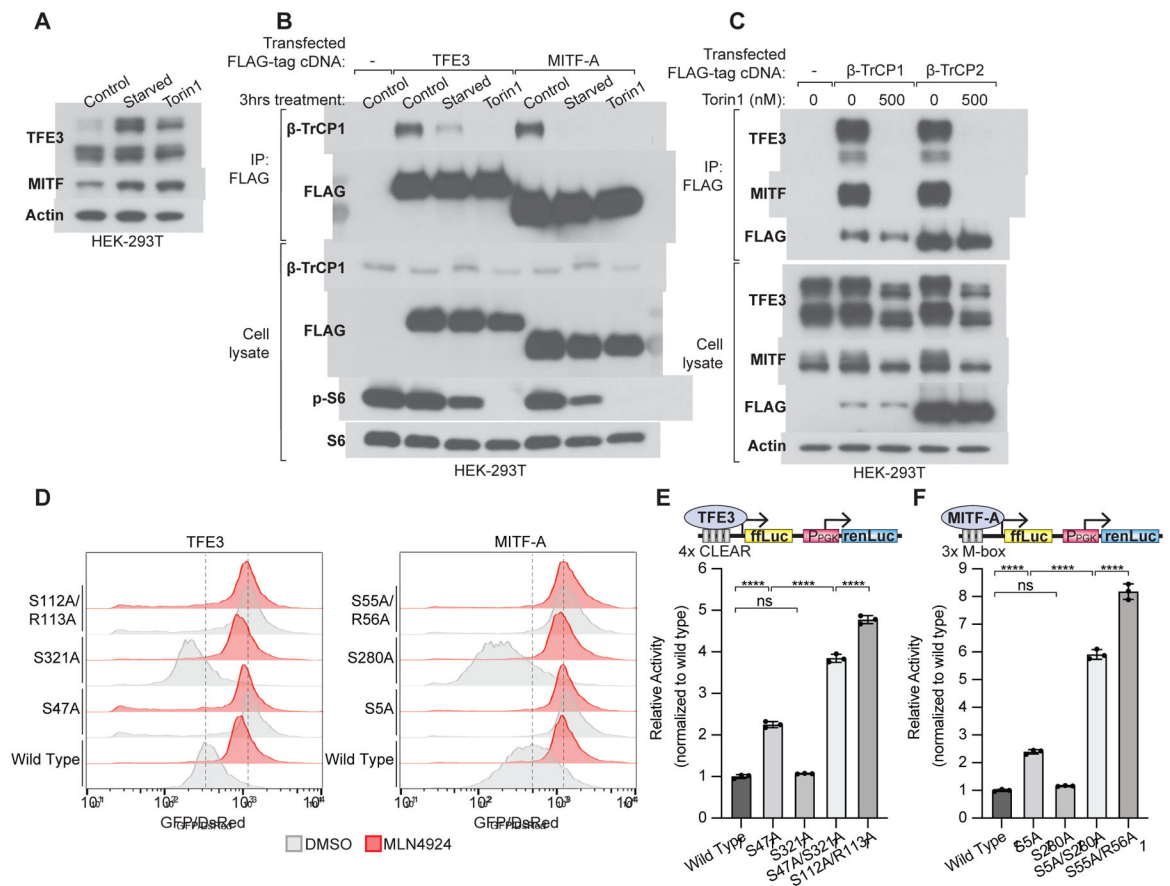
Figure 5. Control of TFE3 and MITF-A degradation by nutrients is crucial to suppress transcriptional activity.

(A) Immunoblotting in HEK-293T cells starved of amino acids/serum or treated with 500 nM Torin1 for 24 hours.

(B) Immunoblotting from anti-FLAG immunoprecipitates of transfected FLAG-tagged TFE3 or MITF-A with amino acid/serum starvation or 500 nM Torin1 for 3 hours.

(C) Immunoblotting from anti-FLAG immunoprecipitates of transfected FLAG-tagged β-TrCP1/2 in the presence of 1 μM MLN4924, −/+ 500 nM Torin1, for 12 hours.

(D) Flow cytometry analysis of HEK-293T cells stably expressing GPS TFE3 or MITF-A reporters −/+ 1 μM MLN4924.

(E) A dual luciferase reporter was stably expressed in TFE3/MITF double KO HEK-293T cells. The *ff*Luciferase is under the expression of 4xCLEAR motif while the *ren*Luciferase internal control is expressed under a constitutive PGK promoter; the ratio of *ff*Luciferase/*ren*Luciferase determines the relative transcriptional activity. Complementation of wild type and mutant TFE3 was achieved by lentiviral stable expression and the relative activity was determined by obtaining the ratio of luminescence. **(F)** Same assay as (E) but utilizing a 3xM-box motif to determine the activity of MITF-A following complementation of wild type and mutant MITF-A constructs in TFE3/MITF double KO HEK-293T cells. Data was analyzed using an ordinary one-way ANOVA followed by Tukey's multiple comparisons test where **** represents a P-value 0.0001 and ns represents not passing statistical significance (P > 0.05). Plotted is the standard deviation from biological replicates.
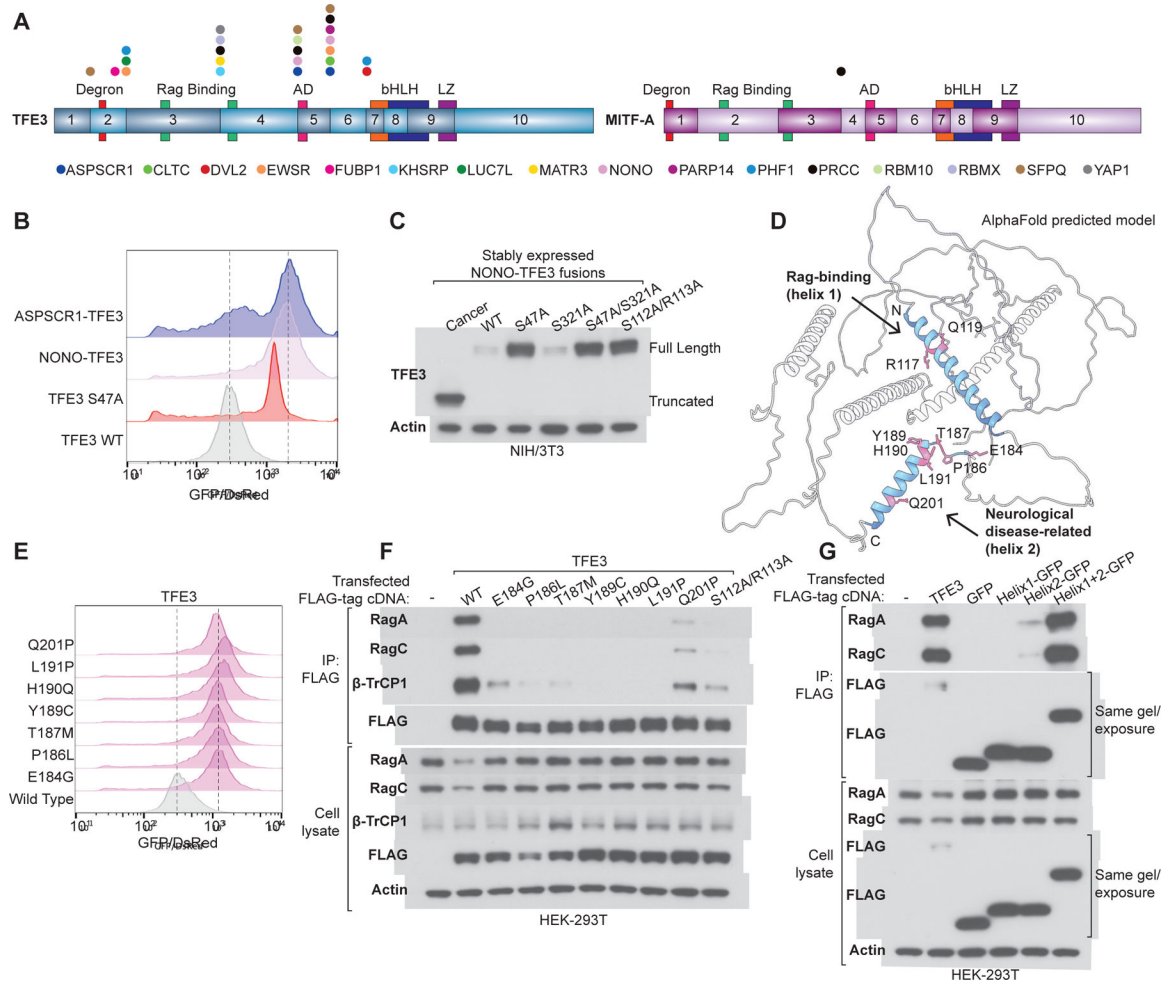
Figure 6. TFE3 is aberrantly stabilized in translocation renal cell carcinoma and a neurodevelopmental syndrome.

(A) Schematic of clinically reported oncogenic TFE3 and MITF fusion proteins, highlighting the β-TrCP1/2 degron, the two helices required for Rag binding, the activation domain (AD), and the basic helix-loop-helix leucine zipper (bHLH-LZ) required for DNA binding. The position of each partner represents the breakpoint site where the C-terminal portion of the transcription factor is fused to the N-terminal portion of the partner. The fusion boundaries were extracted from the primary literature.[44–64]

(B) Flow cytometry analysis of HEK-293T cells stably expressing GPS TFE3 reporters.

(C) Immunoblotting from cell lysates of NIH/3T3 expressing various NONO-TFE3 fusions, where cancer denotes the truncated fusion observed in the clinic, and full-length represents the entire coding sequence of TFE3 fused to the truncated NONO.

(D) Predicted structure of TFE3 by AlphaFold, highlighting two helices and the neurological disease associated residues in pink. Image generated using ChimeraX.

(E) Flow cytometry analysis of HEK-293T stably expressing GPS TFE3 variants.

(F) Immunoblotting from anti-FLAG immunoprecipitates of transfected FLAG-tagged TFE3 variants.

(G) Immunoblotting from anti-FLAG immunoprecipitates of transfected FLAG-tagged TFE3 or GFP fusions. Helix1 represents amino acids 106–140, Helix2 180–210, and Helix1+2 106–210 of TFE3.
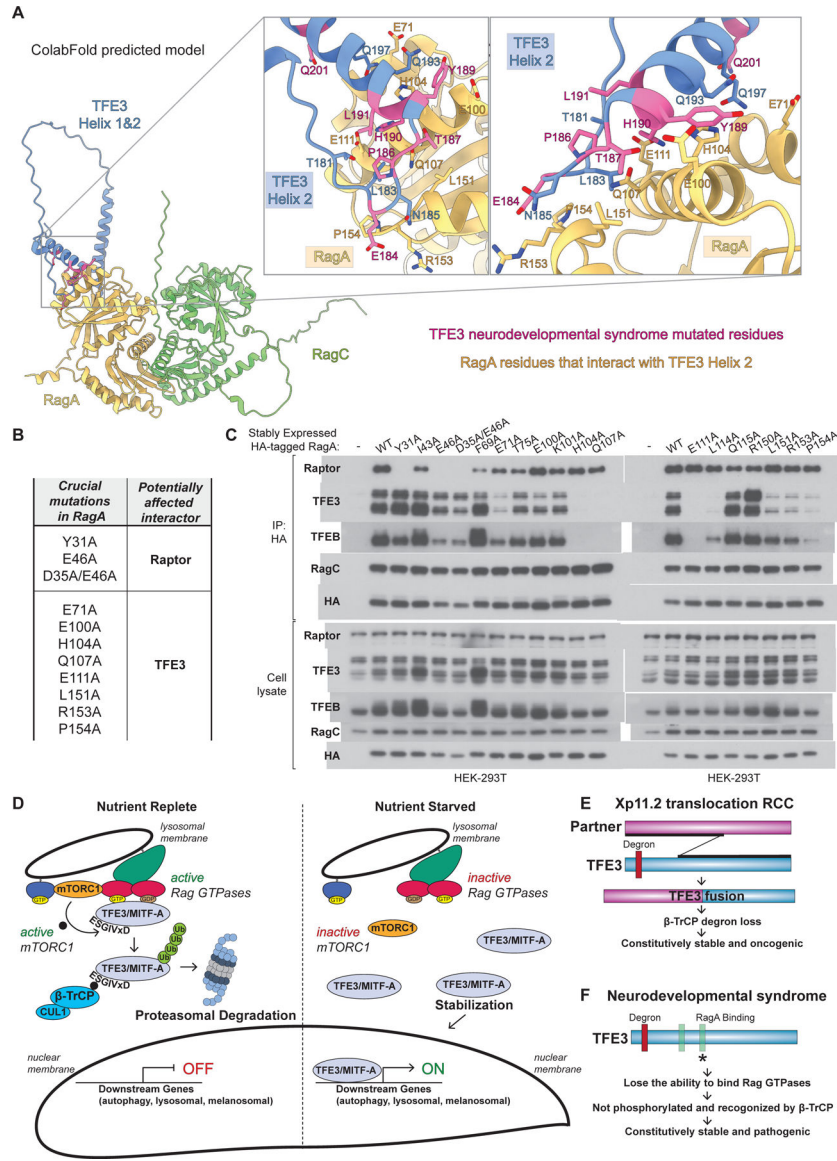
Figure 7. The MiT/TFE family docks directly onto RagA.

(A) A ColabFold structure prediction of TFE3 (amino acids 106–210) and RagA/C reveals an interface between RagA and TFE3. The structure prediction was performed using the AlphaFold structure prediction tool within ChimeraX by directly inputting the amino acid sequences of TFE3 and RagA/C.

(B) Summary of the residues within RagA that are known or predicted to make direct contacts with Raptor or TFE3, respectively.

(C) Immunoblotting from anti-HA immunoprecipitates of HA-tagged RagA variants stably expressed in RagA/B KO cells.

(D) Model demonstrating a central role for regulated protein stability in the control of TFE3 and MITF transcriptional activity by nutrients.

(E) The β-TrCP1/2 degron within TFE3 is recurrently lost in translocation renal cell carcinoma.

(F) Missense mutations within a hotspot region constitutively stabilize TFE3 by abrogating the interaction interface with Rag GTPases, causing a severe neurodevelopmental syndrome.

KEY RESOURCES TABLE

REAGENT or RESOURCE	SOURCE	IDENTIFIER
Antibodies		
Rabbit polyclonal anti-TFE3	Sigma-Aldrich	HPA023881
Rabbit monoclonal anti-MITF	Cell Signaling Technology	97800
Rabbit polyclonal anti-TFEB	Cell Signaling Technology	4240
Rabbit monoclonal anti-Actin	Cell Signaling Technology	4970
Rabbit monoclonal anti-β-TrCP	Cell Signaling Technology	4394
Rabbit monoclonal anti-FLAG	Cell Signaling Technology	14793
Mouse monoclonal anti-FLAG	Sigma-Aldrich	F1804
Rabbit monoclonal anti-HA	Cell Signaling Technology	3724
Rabbit monoclonal anti-RagA	Cell Signaling Technology	4357
Rabbit polyclonal anti-RagC	Cell Signaling Technology	3360
Rabbit monoclonal anti-LAMTOR1	Cell Signaling Technology	8975
Rabbit monoclonal anti-S6 Ribosomal Protein	Cell Signaling Technology	2217
Rabbit polyclonal anti-Phospho-S6 Ribosomal Protein	Cell Signaling Technology	2211
Rabbit polyclonal anti-Raptor	Sigma-Aldrich	09–217
Rabbit monoclonal anti-His tag	Cell Signaling Technology	12698
Goat anti-Rabbit IgG (H+L) Secondary Antibody, HRP conjugate	Thermo Fisher Scientific	31460
Goat anti-Mouse IgG (H+L) Secondary Antibody, HRP conjugate	Thermo Fisher Scientific	31430
Bacterial and virus strains		
rEcoliXpS	71	NA
Chemicals, peptides, and recombinant proteins		
MLN4924	Selleckchem	S7109
Bortezomib	APExBIO	A2614
Torin1	TOCRIS	4247
p-IκBα peptide: Acetyl-KERLLDDRHD(pS)GLD(pS)MRDEERRASY	Macromolecular Synthesis Lab, St. Jude	NA
TFE3 peptide: LLPESGIVADIELENVLDPDSFYELK	Elim Biopharmaceuticals, Inc.	NA
p-TFE3 peptide: LLPE(pS)GIVADIELENVLDPDSFYELK	Elim Biopharmaceuticals, Inc.	NA

REAGENT or RESOURCE	SOURCE	IDENTIFIER
TFE3 peptide-biotin: LLPESGIVADIELENVLDPDSFYELK-biotin	Elim Biopharmaceuticals, Inc.	NA
p-TFE3-peptide biotin: LLPE(pS)GIVADIELENVLDPDSFYELK-biotin	Elim Biopharmaceuticals, Inc.	NA
MITF-A peptide: AGTMQSESGIVPDFEVGEEFHEEPK	Elim Biopharmaceuticals, Inc.	NA
p-MITF-A peptide: AGTMQSE(pS)GIVPDFEVGEEFHEEPK	Elim Biopharmaceuticals, Inc.	NA
MITF-A peptide-biotin: MQSESGIVPDFEVGEEFHEEPK-biotin	Elim Biopharmaceuticals, Inc.	NA
p-MITF-A peptide-biotin: MQSE(pS)GIVPDFEVGEEFHEEPK-biotin	Elim Biopharmaceuticals, Inc.	NA
Recombinant native MITF-A	This study	NA
Recombinant pS5-MITF-A	This study	NA
Sequencing Grade Trypsin	Promega	V5113
Critical commercial assays		
Gentra Puregene Cell Kit	QIAGEN	158767
Dual Luciferase Reporter Assay System	Promega	E1910
Polyjet Transfection Reagent	SignaGen	SL100688
Lipofectamine RNAiMAX	Thermo Fisher Scientific	13778075
Q5 Site Directed Mutagenesis kit	New England Biolabs	E0554S
Fe-NTA IMAC beads	Cell Signaling Technology	20432S
S-Trap Micro Proteomics Sample Prep Columns	Protifi, LLC	C02-micro-10
RNeasy Plus Mini kit	Qiagen	74134
iScript cDNA Synthesis kit	BioRad	1708891
Platinum SYBR Green qPCR Supermix-UDG	Thermo Fisher Scientific	11733038
Deposited data		
Raw images and mass spectrometry files	This study	https://doi.org/ 10.17632/sbmzjr7nx3.1
Experimental models: Cell lines		
HEK-293T	ATCC	CRL-3216
NIH/3T3	ATCC	CRL-1658
ARPE-19	ATCC	CRL-2302
Oligonucleotides		
4xCLEAR: GTAGGCCACGTGACCGGGGTAGGCCACGTGACCGGGGTAGGCCACGTGACCGGGGTAGGCCACGTGACCGGGC	Integrated DNA Technologies	NA
3xM-box: AAAAGTCAGTCATGTGCTTTTCAAAAGTCAGTCATGTGCTTTTCAAAAGTCAGTCATGTGCTTTTC	Integrated DNA Technologies	NA

REAGENT or RESOURCE	SOURCE	IDENTIFIER
sgTFE3 – GTTCATCGAGGGTCTTGCTG	Integrated DNA Technologies	NA
sg1-MITF – GCCACATACAGCAAGCCCAA	Integrated DNA Technologies	NA
sg2-MITF – GGTACCTTAAGGACTTCCAT	Integrated DNA Technologies	NA
Recombinant DNA		
pHAGE GPS 3.0 DEST	27	NA
pHAGE FLAG-HA DEST	27	NA
pHAGE EF1α DEST	72	NA
pHAGE-5xISRE-ffLuc-PGK-renLuc	73	NA
TFE3 Ultimate ORF Collection Entry Clone	Thermo Fisher Scientific	IOH14020
MITF-A Ultimate ORF Collection Entry Clone	Thermo Fisher Scientific	IOH52183
β-TrCP1 Ultimate ORF Collection Entry Clone	Thermo Fisher Scientific	IOH11366
β-TrCP2 Ultimate ORF Collection Entry Clone	Thermo Fisher Scientific	IOH11042
Lenti CRISPR v2	Addgene	52961
SupD	Addgene	68307
SepOTSλ	Addgene	68292
Barcoded GPS-ORFeome expression library	27	NA
Ubiquitome sgRNA CRISPR-Cas9 Library	74	NA
Genome-wide sgRNA CRISPR-Cas9 Root Library	75	NA
Software and algorithms		
Bowtie 2	76,77	http://bowtie-bio.sourceforge.net/index.shtml
Cutadapt	78	https://cutadapt.readthedocs.io/en/stable/index.html
MAGeCK	79	https://sourceforge.net/projects/mageck/
FlowJo	FlowJo	https://www.flowjo.com/
AlphaFold	65,80	https://alphafold.ebi.ac.uk/
ColabFold	66	Access via ChimeraX
ChimeraX	81,82	https://www.rbvi.ucsf.edu/chimerax/
NEBaseChanger	NEBaseChanger	https://nebasechanger.neb.com/
PEAKS X+	Bioinformatics Solutions, Inc.	https://www.bioinfor.com/peaks-studio-x-plus/
Jalview	83	https://www.jalview.org/

REAGENT or RESOURCE	SOURCE	IDENTIFIER
GraphPad Prism version 9	GraphPad Prism version 9	https://www.graphpad.com/
Other		
Non-targeting Control 1 siRNA	Dharmacon	D-001810-01-05
Non-targeting Control 2 siRNA	Dharmacon	D-001810-02-05
Non-targeting Control 3 siRNA	Dharmacon	D-001810-03-05
β-TrCP1 1 siRNA	Dharmacon	J-003463-05-0005
β-TrCP1 2 siRNA	Dharmacon	J-003463-06-0005
β-TrCP1 3 siRNA	Dharmacon	J-003463-07-0005
β-TrCP2 1 siRNA	Dharmacon	J-003490-05-0005
β-TrCP2 2 siRNA	Dharmacon	J-003490-06-0005
β-TrCP2 3 siRNA	Dharmacon	J-003490-07-0005